



TRABAJO FIN DE MÁSTER / MASTER AMAIERAKO LANA /
FINAL MASTER'S DISSERTATION

S-CO₂ FOR EFFICIENT POWER GENERATION WITH ENERGY STORAGE

MARTA CERIO VERA

Máster Universitario en Ingeniería Industrial / Industria Ingeniaritza
Unibertsitate Masterra / Master in Industrial Engineering
&
MSc in Energy Systems and Thermal Processes

Director / Zuzendaria / Supervisor: Dr. Kumar Patchigolla

2015 - 2016

CRANFIELD UNIVERSITY

MARTA CERIO VERA

S-CO₂ FOR EFFICIENT POWER GENERATION WITH ENERGY
STORAGE

SCHOOL OF ENERGY, ENVIRONMENT AND AGRIFOOD
MSc in Energy Systems and Thermal Processes

MASTER OF SCIENCE
Academic Year: 2015 - 2016

Supervisor: Kumar Patchigolla
September 2016

CRANFIELD UNIVERSITY

SCHOOL OF ENERGY, ENVIRONMENT AND AGRIFOOD
MSc in Energy Systems and Thermal Processes

MASTER OF SCIENCE

Academic Year 2015 - 2016

MARTA CERIO VERA

S-CO₂ for Efficient Power Generation with Energy Storage

Supervisor: Kumar Patchigolla
September 2016

This thesis is submitted in partial fulfilment of the requirements for
the degree of Master of Science

© Cranfield University 2016. All rights reserved. No part of this
publication may be reproduced without the written permission of the
copyright owner.

ABSTRACT

Supercritical CO₂ (s-CO₂) power cycle has gained interest for concentrating solar power (CSP) application in the last decade to overcome the current low efficiency and high costs of the plants. This cycle is a potential option to replace the steam Rankine cycle due to its higher efficiency, more compact turbomachinery and possibility of including heat storage and direct heating. The purpose of this project is to determine the suitability of integrating s-CO₂ power cycle into CSP plants with energy storage.

With this aim, recompression and partial cooling cycles were identified as appropriate s-CO₂ cycle configurations for CSP application. They were modelled, optimised and compared for scenarios that represent different types of CSP plants and operating conditions. The selection of scenarios includes current technologies (parabolic trough and central tower), as well as a direct heating modular system with wet and dry cooling. The partial cooling cycle presented advantages for CSP applications in the four scenarios considered, therefore, it was implemented as the power cycle in the CSP plant.

The simulation of the s-CO₂ cycle CSP plants corresponding to each scenario revealed that s-CO₂ cycle plants could exceed the efficiency of existing Rankine cycle plants when using central tower or direct heating technologies, but not with parabolic trough. In addition, it was demonstrated that the use of wet cooling with s-CO₂ power cycle results contrary to the requirements of water consumption minimisation in CSP plants since a higher amount of cooling water than in current plants was demanded. Therefore, the highest potential was shown by CSP plants that use direct heating of s-CO₂ and dry cooling, obtaining a high efficiency close to 45% and reducing greatly the utilisation of water.

(7994 words)

Keywords:

CSP, Recompression, Partial Cooling, Dry Cooling, Thermoflex.

ACKNOWLEDGEMENTS

First of all, I would like to thank my supervisor, Dr. Kumar Patchigolla, for his support and guidance during the realisation of this project. Special thanks are also addressed to Dr. Peter Turner for his recommendations and expertise in CSP plants.

I am also very grateful to Pablo Ramos, who worked also in CSP plant modelling, for his help and advice with Thermoflex software.

Additionally, I want to show gratitude to the Escuela Técnica Superior de Ingeniería de Bilbao for giving me the opportunity to come to Cranfield University and complete my education.

Finally, I would like to dedicate this thesis to my parents, my brother and Bernal because they always support me unconditionally.

TABLE OF CONTENTS

ABSTRACT	i
ACKNOWLEDGEMENTS.....	iii
LIST OF FIGURES.....	vi
LIST OF TABLES	vii
LIST OF EQUATIONS.....	viii
LIST OF ABBREVIATIONS	ix
NOMENCLATURE	x
1 INTRODUCTION.....	3
1.1 Context	3
1.2 S-CO ₂ Power Cycle.....	4
1.3 S-CO ₂ Cycle Integration in CSP Plants.....	6
1.4 Aims and Objectives	7
2 MATERIALS AND METHODS.....	9
2.1 Selection of Software	9
2.2 S-CO ₂ Power Cycle Configurations	9
2.3 S-CO ₂ Power Cycles Modelling	11
2.3.1 Models of Recompression and Partial Cooling Cycles	11
2.3.2 Optimisation of Recompression and Partial Cooling Cycles.....	13
2.3.3 Validation of Models	14
2.4 Selection of Scenarios	15
2.5 CSP Plant Modelling.....	17
3 RESULTS AND DISCUSSION	19
3.1 Optimisation of Recompression and Partial Cooling Cycles	19
3.2 Comparison of Recompression and Partial Cooling Cycles.....	21
3.3 Comparison of S-CO ₂ Cycle CSP Plants with Current Plants.....	23
3.3.1 Net Plant Efficiency	23
3.3.2 Cooling Fluid Flowrate.....	24
3.3.3 Thermal Energy Storage System Size	26
4 CONCLUSIONS AND RECOMMENDATIONS	29
REFERENCES.....	33
APPENDICES	37
Appendix A S-CO ₂ Power Cycle Layouts.....	37
Appendix B Discretisation of Heat Exchangers.....	42
Appendix C Code Implemented in EES	44
Appendix D Models of CSP Plants in Thermoflex.....	51
Appendix E Receiver for Direct Heating of s-CO ₂	55

LIST OF FIGURES

Figure 1. Thermal efficiencies of power systems and applications [1].....	3
Figure 2. Simple recuperated Brayton cycle [9].....	5
Figure 3. CO ₂ specific heat as function of temperature and pressure [13]	5
Figure 4. Recompression cycle with reheating [11].....	10
Figure 5. Partial cooling cycle with reheating [11]	10
Figure 6. Parabolic trough CSP plant [22]	15
Figure 7. Central tower CSP plant [22].....	16
Figure 8. Modular tower receiver with s-CO ₂ Brayton cycle [8]	16
Figure 9. Net efficiency of current and s-CO ₂ cycle CSP plants	23
Figure 10. Temperature profile in the intercooler of scenario 2 for the minimum cooling water flowrate	25
Figure 11. Comparison of cooling fluid flowrate of current and s-CO ₂ cycle CSP plants	26
Figure A-1. Simple recuperated Brayton Cycle [4]	37
Figure A-2. Reheated Brayton cycle [4].....	38
Figure A-3. Intercooled Brayton cycle [4]	39
Figure A-4. Precompression cycle [7].....	40
Figure A-5. Recompression cycle [7].....	40
Figure A-6. Partial cooling cycle [7]	41
Figure A-7. Discretisation of a counter-flow heat exchanger into sub-heat exchangers	42
Figure A-8. Model of parabolic trough CSP plant with s-CO ₂ partial cooling cycle in Thermoflex (scenario 1)	51
Figure A-9. Model of central tower CSP plant with s-CO ₂ partial cooling cycle in Thermoflex (scenario 2).....	52
Figure A-10. Model of modular tower CSP plant with wet cooling and s-CO ₂ partial cooling cycle in Thermoflex (scenario 3).....	53
Figure A-11. Model of modular tower CSP plant with dry cooling and s-CO ₂ partial cooling cycle in Thermoflex (scenario 4).....	54

LIST OF TABLES

Table 1. Validation cases conditions [10, 11]	14
Table 2. Validation results	14
Table 3. Scenarios conditions	17
Table 4. Optimisation results for maximum efficiency	19
Table 5. Optimisation results for scenario 1 and scenario 2 recompression cycle	20
Table 6. Comparison of recompression and partial cooling cycles results	21
Table 7. Cooling fluid flowrates	25
Table 8. Tanks volume of current and s-CO ₂ cycle CSP plants	26
Table A-1. Tubes parameters [25].....	55
Table A- 2. Pressure drops in heaters of scenario 3 and 4	56

LIST OF EQUATIONS

(2-1).....	11
(2-2).....	12
(2-3).....	12
(2-4).....	13
(2-5).....	13
(A-1)	42
(A-2)	42
(A-3)	42
(A-4)	43
(A-5)	43
(A-6)	43
(A-7)	43
(A-8)	43
(A-9)	55

LIST OF ABBREVIATIONS

CIT	Compressor Inlet Temperature
CSP	Concentrating Solar Power
EES	Engineering Equation Solver
HPT	High Pressure Turbine
HTF	Heat Transfer Fluid
HTR	High Temperature Recuperator
HX	Heat Exchanger
LPT	Low Pressure Turbine
LTR	Low Temperature Recuperator
MC	Main Compressor
PC	Precompression Compressor
PR	Pressure Ratio
RC	Recompression Compressor
RPR	Ratio of Pressure Ratios
s-CO ₂	Supercritical Carbon Dioxide
TES	Thermal Energy Storage
TIT	Turbine Inlet Temperature

NOMENCLATURE

c	Specific Heat (kJ/kgK)
\dot{C}	Heat Capacity (kJ/K)
D	Internal Diameter (m)
h	Enthalpy (kJ/kg)
f	Friction factor
L	Length covered in the Receiver (m)
\dot{m}	Mass Flowrate (kg/s)
N	Number of Sub-heat Exchangers
NTU	Number of Transfer Units
P	Pressure (MPa)
\dot{Q}	Heat Transfer Rate (kW)
T	Temperature (°C)
ΔT	Temperature Difference (°C)
UA	Heat Exchanger Conductance (kW/K)
v	Velocity (m/s)
\dot{W}	Power (kW)
ε	Heat Exchanger Effectiveness (%)
η_C	Compressor Isentropic Efficiency (%)
η_T	Turbine Isentropic Efficiency (%)
η_{th}	Thermal Efficiency (%)
ρ	Density (kg/m ³)

S-CO₂ FOR EFFICIENT POWER GENERATION WITH ENERGY STORAGE

Marta Cerio Vera

School of Energy, Environment and Agrifood, Cranfield University, Cranfield, Bedfordshire, MK34 0AL

Supervisor: Kumar Patchigolla

ABSTRACT

Supercritical CO₂ (s-CO₂) power cycle has gained interest for concentrating solar power (CSP) application in the last decade to overcome the current low efficiency and high costs of the plants. This cycle is a potential option to replace the steam Rankine cycle due to its higher efficiency, more compact turbomachinery and possibility of including heat storage and direct heating. The purpose of this project is to determine the suitability of integrating s-CO₂ power cycle into CSP plants with energy storage.

With this aim, recompression and partial cooling cycles were identified as appropriate s-CO₂ cycle configurations for CSP application. They were modelled, optimised and compared for scenarios that represent different types of CSP plants and operating conditions. The selection of scenarios includes current technologies (parabolic trough and central tower), as well as a direct heating modular system with wet and dry cooling. The partial cooling cycle presented advantages for CSP applications in the four scenarios considered, therefore, it was implemented as the power cycle in the CSP plant.

The simulation of the s-CO₂ cycle CSP plants corresponding to each scenario revealed that s-CO₂ cycle plants could exceed the efficiency of existing Rankine cycle plants when using central tower or direct heating technologies, but not with parabolic trough. In addition, it was demonstrated that the use of wet cooling with s-CO₂ power cycle results contrary to the requirements of water consumption

minimisation in CSP plants since a higher amount of cooling water than in current plants was demanded. Therefore, the highest potential was shown by CSP plants that use direct heating of s-CO₂ and dry cooling, obtaining a high efficiency close to 45% and reducing greatly the utilisation of water.

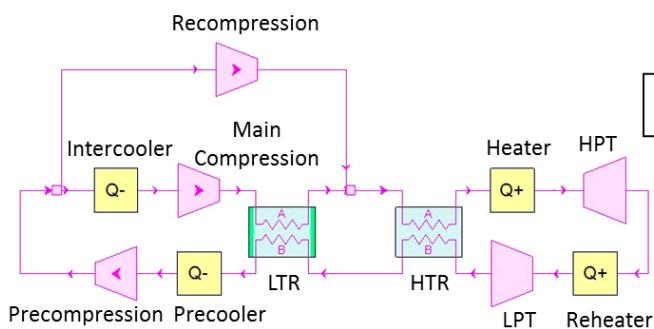
(7994 words)

Keywords:

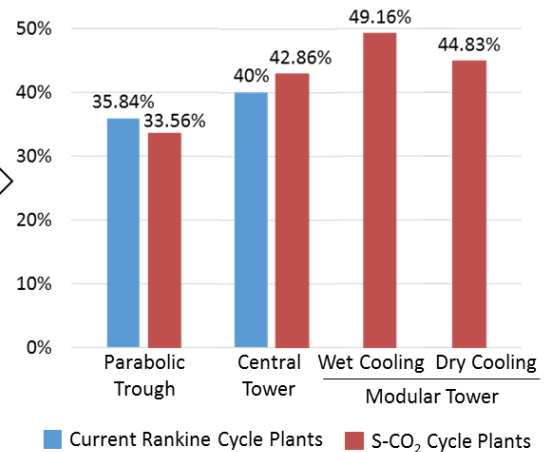
CSP, Recompression, Partial Cooling, Dry Cooling, Thermoflex.

GRAPHICAL ABSTRACT

S-CO₂ Partial Cooling Cycle



Net Efficiency of CSP Plants



1 INTRODUCTION

1.1 Context

Supercritical CO₂ (s-CO₂) power cycle has gained interest for different applications during the last two decades due to its potential advantages over conventional power technologies. The main benefits of s-CO₂ Brayton cycle are high thermal efficiency, compact turbomachinery, simple layout and reduced plant size. The cycle can be considered an alternative to the steam Rankine cycle for mild inlet turbine temperatures (500-800°C), as shown in Figure 1. Therefore, its application covers a wide range including nuclear, fossil fuels, exhaust/waste heat recovery and renewable (solar, geothermal and fuel cells) [1].

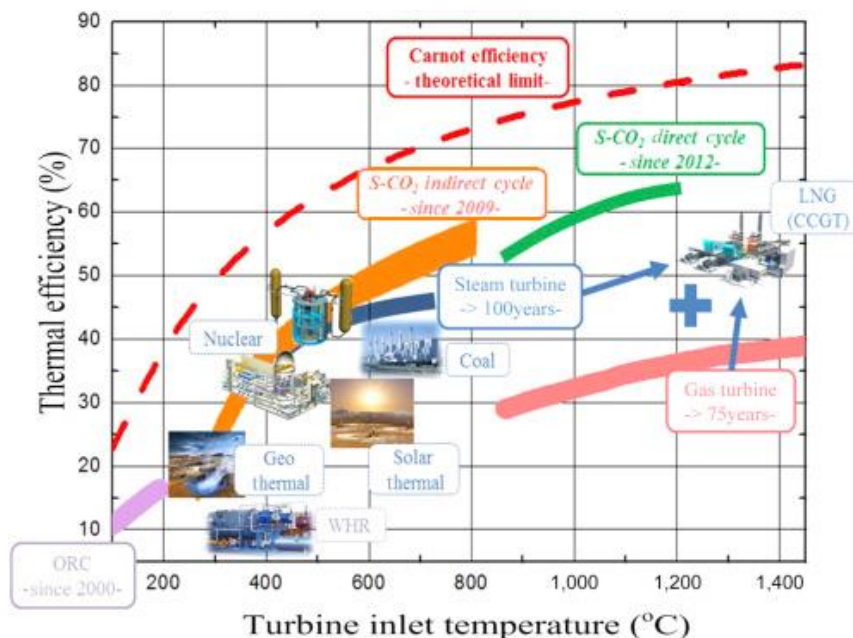


Figure 1. Thermal efficiencies of power systems and applications [1]

Carbon dioxide was suggested by Feher [2] as an optimum working fluid for the supercritical cycle because its critical point is reached at moderate conditions (30.98°C, 7.38 MPa), it is stable and inert in the temperature range of interest, abundant, relatively cheap, non-toxic and has well-known properties. Although the s-CO₂ cycle and its advantages have been known since the late 1960's [2, 3], it is still in a demonstration stage and it had never been implemented in practice until few years ago [4, 5] due to technical challenges. Some reasons were the high pressure required and the lack of an appropriate heat source, compact heat

exchangers and turbomachinery for a supercritical fluid [6]. Studies on s-CO₂ cycle have been revitalised in the last two decades, mainly focusing on applications for Generation IV nuclear reactors [6, 7]. More recently, interest in deployment for concentrating solar power (CSP) plants has grown to overcome their current low efficiency and high costs [8-12].

S-CO₂ Brayton cycle is a potential option to increase CSP plants efficiency at the same time as being simple and capable of integrating heat storage. In comparison with steam Rankine cycles used in CSP plants, it provides higher temperature operation and efficiency at temperatures achievable with current collector technologies (500-800°C). In addition, the smaller volume of the plant (approximately 4 times) and power blocks (approximately 10 times for the turbomachinery that has fewer stages) can reduce installation, maintenance and operation costs. Compared to an air- or helium- Brayton cycle, it achieves better efficiency at much lower temperature [1, 9-11].

CSP plants currently utilise thermal oil, molten salts or water/steam as the heat transfer fluid (HTF), whose properties represent the main constraint of plants performance. The use of thermal oil (usual in parabolic trough plants) is limited to 400°C and molten salts (power tower plants) to 590°C due to material degradation, while direct steam generation means complex controls and limitation of heat storage integration. Increasing the operating temperature of the HTF would involve a higher cycle efficiency and more efficient heat storage. Some proposed HTF options to reach higher temperatures are direct heating of air and s-CO₂, both being the working fluid of the power cycle [9, 10].

1.2 S-CO₂ Power Cycle

The s-CO₂ cycle is a closed Brayton cycle where the CO₂ is above its critical temperature and pressure. The basic layout is the simple recuperated Brayton cycle (Figure 2). A process of heat recuperation is required to achieve high thermal efficiency by minimising waste heat. The CO₂ does not behave like an ideal gas near to the critical point and its properties are significantly affected by pressure and temperature. However, the cycle takes advantage of this real gas behaviour in order to obtain high efficiency and compact turbomachinery.

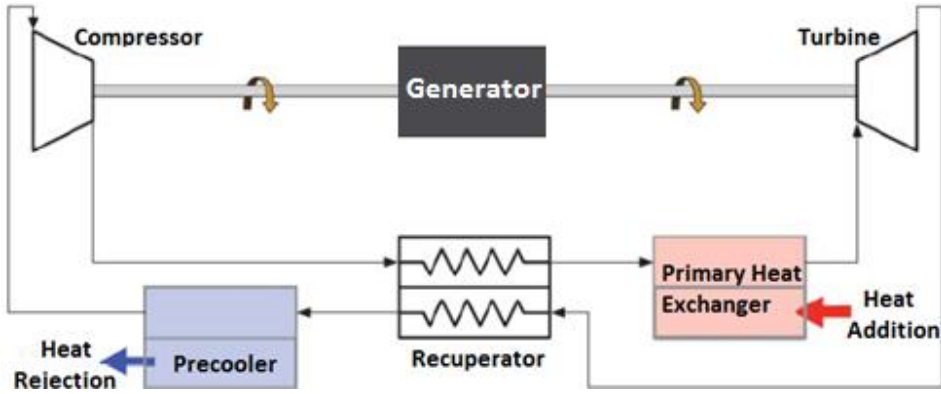


Figure 2. Simple recuperated Brayton cycle [9]

The main way to increase cycle efficiency is to perform compression close to the critical point because it results in a considerable reduction of compressor work in comparison with an ideal gas Brayton cycle. The reason of this is the low compressibility of CO₂ at the critical point. The compact turbomachinery is a result of the fluid remaining dense throughout the whole cycle since the minimum pressure in the supercritical cycle corresponds to the critical one (7.38 MPa) [6].

The real gas behaviour of the s-CO₂ also introduces a possible pinch-point problem in the recuperator. A pinch point is the location of a minimum temperature difference in a heat exchanger. Due to the strong variation of specific heat and thus heat capacity with temperature and pressure (Figure 3), the temperature difference between the recuperator streams varies strongly. For certain operating conditions the pinch-point problem occurs if a minimum temperature difference is achieved along the recuperator and not at the inlet or outlet [6].

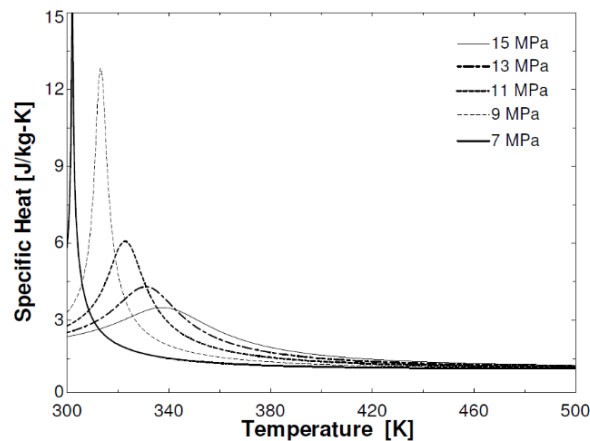


Figure 3. CO₂ specific heat as function of temperature and pressure [13]

Although there exist different s-CO₂ cycle layouts, there are multiple variations of the simple recuperated Brayton cycle. Reheating and intercooling stages can be included to improve thermal efficiency. Angelino [3] introduced compound cycles in order to prevent the pinch-point problem and reduce the irreversibilities in the recuperator. Those cycles result in higher efficiency but more complex layouts. The main s-CO₂ cycle layouts are reviewed in Appendix A.

The appropriate s-CO₂ cycle layout changes depending on the energy application because each cycle optimises at a different pressure ratio and undergoes different efficiency trends when varying the operating temperatures. Applications for s-CO₂ are wide and differ in energy source, technology and operating conditions, thus each case must be studied to determine the suitable cycle [14].

1.3 S-CO₂ Cycle Integration in CSP Plants

When considering the incorporation of s-CO₂ power cycle into CSP plants, the capacity of integrating dry cooling and heat storage must be taken into account.

Unlike other traditional power applications CSP plants are typically built in arid regions where water scarcity exists. Therefore, dry cooling is preferred to minimise water consumption. However, s-CO₂ cycles have maximum efficiency when the compressors operate near to the critical temperature (31°C), which is possible with wet cooling but not with dry cooling at desert air temperatures. Reduced efficiency, larger heat exchangers and temperature difference between air and working fluid are the main disadvantages of dry cooling [9, 10].

Thermal energy storage (TES) is essential to increase CSP plant capacity factor and mitigate the effects of the solar resources intermittency. Charging energy storage devices at sunlight periods allows for power production when there are transient clouds and at night. Molten salts are the most mature heat storage technology for CSP plants and, in the case of s-CO₂ direct heating, they are a feasible option to store heat transferred from s-CO₂ due to its single phase operation [10, 15]. However, current TES materials limit the temperature of storage and consequently would reduce the efficiency benefit of using s-CO₂ as the HTF.

1.4 Aims and Objectives

The aim of this project is to determine the suitability of integrating s-CO₂ power cycle into CSP plants with energy storage.

The main objectives to fulfil the project aim are the following:

- Identify appropriate s-CO₂ cycle layouts and select different scenarios for the incorporation of s-CO₂ power cycle in CSP plants.
- Define the operation of s-CO₂ power cycles for the operating conditions of each scenario and compare them to select the most appropriate configuration for CSP application.
- Determine the performance of the CSP plant using a s-CO₂ power cycle for each scenario.
- Compare the performance and operation parameters of s-CO₂ power cycle CSP plants with those of current CSP plants.

2 MATERIALS AND METHODS

This chapter focuses on describing the methodology employed in this thesis. Firstly, models of s-CO₂ power cycles considered for CSP application were developed and validated against literature data, so that these cycles could be compared in different scenarios. These scenarios represent different types of CSP plants in which a s-CO₂ cycle is used for power production. Each scenario has its own operating conditions and consequently, each power cycle had to be optimised in every case.

Once the optimised s-CO₂ cycles were defined, the most appropriate configuration was selected to be implemented into the corresponding CSP plant. Afterwards, the complete CSP plant of each scenario was modelled adding the solar field, heat storage and cooling process to the s-CO₂ power cycle.

2.1 Selection of Software

Some of the software for modelling thermal processes was considered to model s-CO₂ power cycles for CSP application: Aspen Plus, EES and Thermoflex. The main factor to choose the software was the availability of the properties of s-CO₂ and common HTFs, such as thermal oil and molten salts. The three software packages mentioned include the database REFPROP, which contains CO₂ properties in the range of interest [16].

Regarding CSP application, only Thermoflex incorporates HTFs, solar field and heat storage options. In order to define the s-CO₂ cycles, EES was selected instead of Aspen Plus because it has been used in previous work [9-11] and it is a straightforward tool to optimise the cycle. After this step, Thermoflex was used to model the complete CSP plant.

2.2 S-CO₂ Power Cycle Configurations

The s-CO₂ cycle configurations considered by Turchi and Neises [11] for CSP plants are recompression (Figure 4) and partial cooling (Figure 5) cycles including one stage of reheat, due to their high efficiency and simple layout.

2.3 S-CO₂ Power Cycles Modelling

Models of s-CO₂ recompression and partial cooling cycles were developed in EES, as well as in Thermoflex although the latter software was intended to be used to model the whole CSP plant. The reason for this is to determine any difference in the results obtained with both software. Unless it is specified, same considerations were applied regardless of the software utilised.

2.3.1 Models of Recompression and Partial Cooling Cycles

The models of recompression and partial cooling cycles follow the layout and numbering shown in Figure 4 and Figure 5. The assumptions made to model the cycles are the following:

- Steady-state operation
- Adiabatic components.
- No pressure drops in heat exchangers.
- The intermediate pressure of the stage of reheat is the average of the high and low side pressures.
- The outlet temperature of the recompression compressor (RC) is set to be equal to the cold outlet temperature of the low temperature recuperator (LTR).
- The previous condition determines the value of the split ratio, which represents the mass flowrate through the main compressor (MC) divided by the total mass flowrate.

Both s-CO₂ cycles comprise turbines, compressors, heat exchangers and heat addition or rejection elements, which were modelled as described below.

Turbines and Compressors

The performance of turbines and compressors is calculated with an isentropic model. The isentropic efficiency relates the actual work developed/required and the corresponding maximum isentropic work:

$$\eta_T = \frac{\dot{W}_T}{\dot{W}_{T,s}} = \frac{h_{in} - h_{out}}{h_{in} - h_{out,s}} \quad (2-1)$$

$$\eta_c = \frac{\dot{W}_{C,s}}{\dot{W}_C} = \frac{h_{out,s} - h_{in}}{h_{out} - h_{in}} \quad (2-2)$$

Heat Addition/Rejection

These processes include precooler, intercooler, heater and reheater. The components are considered as heat sources or sinks that allow reaching the CIT in the precooler and intercooler and the TIT in the case of the heater and reheater.

Heat Exchangers

There are two recuperators that exchange heat between the streams of s-CO₂ in counter-flow arrangement. An effectiveness approach is applied to define the performance of the heat exchangers. Since the two recuperators are in series, the effectiveness of the high temperature recuperator (HTR) and the overall hot side are determined, which constrains the effectiveness of the LTR. The effectiveness of a heat exchanger (ε) is defined as the actual heat transfer divided by the maximum theoretical one:

$$\varepsilon = \frac{\dot{Q}}{\dot{Q}_{max}} = \frac{h_{H,in} - h_{H,out}}{h_{H,in} - h(T_{C,in}, P_{H,out})} \quad (2-3)$$

A minimum temperature difference between the hot and cold streams of the recuperators is also established.

After determining the properties of the inlet and outlet streams with the effectiveness, a discretisation of heat exchangers is required in order to evaluate locally the temperature difference across the recuperators and ensure that a pinch-point problem does not happen due to the significant variation of specific heat with temperature and pressure. The discretisation method implemented in EES consists in dividing the heat exchanger into N sub-heat exchangers, so that the changes in s-CO₂ properties are considered and the ε -NTU method becomes more valid for small sub-heat exchangers than for the whole heat exchanger. This division into sub-heat exchangers implies that they exchange an equal amount of heat. The methodology is developed according to Nellis and Klein [17] but applied to a heat exchanger with counter-flow configuration (Appendix B).

With respect to Thermoflex, the component used for heat exchangers is ‘General HX’, which produces temperature profiles that take into account changes in specific heat. In the case of conditions near critical ones, the software follows the previous methodology dividing the process in zones of equal heat exchange [18].

2.3.2 Optimisation of Recompression and Partial Cooling Cycles

The optimisation of recompression and partial cooling cycles was performed in EES for maximum efficiency. The thermal efficiency of these cycles is determined by the net power obtained (expansion work minus compression work) divided by the total heat input from the heater and reheater.

With the aim of determining the operation of the cycles, some parameters were optimised for maximum efficiency. In the case of the recompression cycle, the only variable to optimise was the pressure ratio, while for the partial cooling cycle there were two; the pressure ratio and the ratio of pressure ratios. The pressure ratio (PR) is the relation between the maximum and minimum pressures:

$$PR = \frac{P_{max}}{P_{min}} \quad (2-4)$$

The ratio of pressure of ratios (RPR) determines the intermediate precompression pressure in the partial cooling cycle:

$$RPR = \frac{P_{max}/P_{intermediate} - 1}{P_{max}/P_{min} - 1} \quad (2-5)$$

The values of the variables that provide the maximum efficiency can be easily obtained with EES function ‘Min/Max’. However, if the minimum temperature difference is not fulfilled or a pinch point happens in the recuperators for those operating conditions, the result has to be excluded. Hence, the effects of the optimisation variables in the occurrence of these problems, as well as in thermal efficiency, were studied for both cycles. The code introduced in EES to study recompression and partial cooling cycles is shown in Appendix C. Once these optimisation variables are defined, they can be introduced in Thermoflex.

2.3.3 Validation of Models

Some cases from Turchi *et al.* [10, 11] were chosen to compare their results with those from the models developed in EES and Thermoflex in order to validate them. The operating conditions of the cases are shown in Table 1.

Table 1. Validation cases conditions [10, 11]

Case	Cycle	CIT	TIT	P_{max}	η_c	η_T	ε	Min ΔT_{HX}
1	Recompression	45°C	700°C	25 MPa	89%	93%	97%	5°C
2		60°C						
3	Partial Cooling	45°C						
4		60°C						
5	Recompression	50°C	650°C					
6	Partial Cooling							

The reason for selecting these cases is that the optimised operation parameters are provided together with the thermal efficiency. In addition, for cases 5 and 6 the conductances of the recuperators (UA) are also calculated. Therefore, these results can be directly compared with the ones obtained from the models in EES and Thermoflex (Table 2), which shows very close agreement. The only remarkable difference appears in the conductance of the recuperators because the heat exchanger model of Thermoflex does not always use the discretisation method.

Table 2. Validation results

Case	Turchi <i>et al.</i>				EES				Thermoflex	
	PR	RPR	UA	η_{th}	PR	RPR	UA	η_{th}	UA	η_{th}
1	2.7	-	-	52.3%	2.65	-	-	52.28%	-	52.28%
2	2.5	-	-	49.7%	2.54	-	-	49.74%	-	49.74%
3	5	0.37	-	52.2%	5.02	0.37	-	52.24%	-	52.24%
4	4.5	0.33	-	50.0%	4.47	0.33	-	49.88%	-	49.88%
5	2.5	-	8.54 MW/K	49.66%	2.53	-	8.53 MW/K	49.66%	8.54 MW/K	49.67%
6	4.55	0.369	4.33 MW/K	49.53%	4.55	0.369	4.30 MW/K	49.53%	4.45 MW/K	49.54%

2.4 Selection of Scenarios

The scenarios contemplated for the incorporation of s-CO₂ cycle in CSP plants include existing commercial technologies, as well as a modular system proposed by Turchi and Ma [8] specifically for this application. In these scenarios, a s-CO₂ cycle is used for power production but at different operating conditions since each case represents a different type of CSP plant.

Among CSP technologies, parabolic trough collectors are the most common and mature concentrating system, followed by the solar central tower. However, this is expected to change since there is a trend towards tower technology because they can operate at higher temperatures. Regarding the use of dish/engine systems and linear Fresnel reflectors, there are few commercial plants [19]. Hence, parabolic trough and central tower were the current technologies selected to be studied with a s-CO₂ cycle, representing scenarios 1 and 2 respectively.

The typical parabolic trough CSP plant (Figure 6) has a capacity of 50 MW, uses thermal oil as HTF, reaching 393°C at the exit of the solar field, and molten salts that are stored in two tanks for TES [19]. As a reference plant for scenario 1, Andasol (Spain) was chosen since it has these characteristics [20, 21].

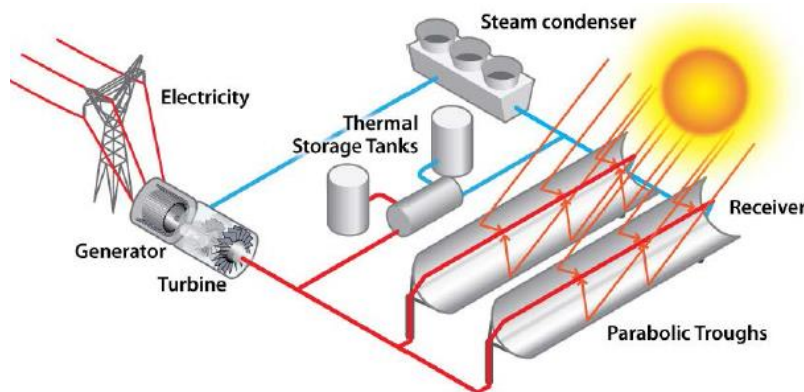


Figure 6. Parabolic trough CSP plant [22]

In central tower CSP plants, molten salts are the most common HTF (reaching 565°C) and can be used as heat storage medium at the same time (Figure 7). Recent projects of large tower plants have been in the region of 100 MW [19]. The representative plant of scenario 2 is Gemasolar (Spain), which was the first central tower CSP plant with molten salts storage [20, 23, 24]. Its power output is

17 MW, therefore the parameters were scaled-up so that they could be compared with those of a 100 MW plant.

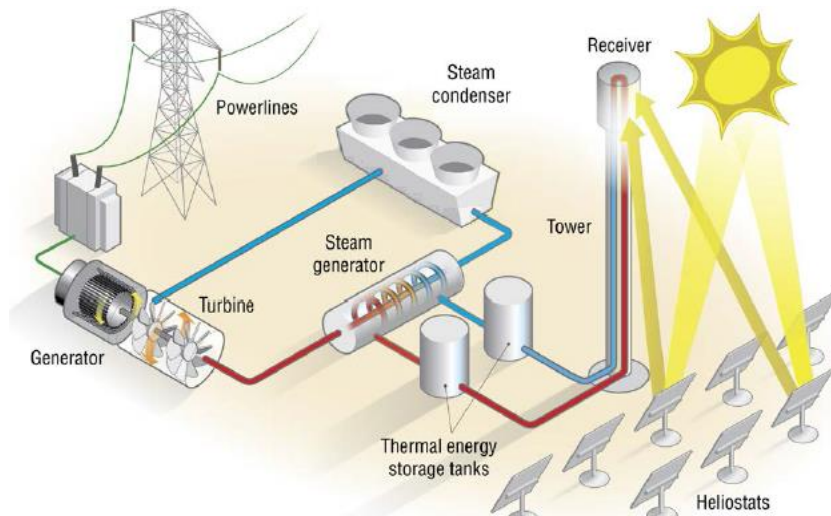


Figure 7. Central tower CSP plant [22]

On the other hand, the proposed modular system [8] is a variation of tower technology (Figure 8). Each tower would have a maximum capacity of 10 MW and its own turbomachinery integrated in the supporting column. The s-CO₂ would be directly heated, reaching temperatures up to 700°C. According to the type of cooling, it was divided into two different scenarios, using water (wet cooling, scenario 3) or air (dry cooling, scenario 4). In these scenarios, heat storage would be desirable but was not considered since it does not exist any commercial TES medium to store heat at such high temperatures.

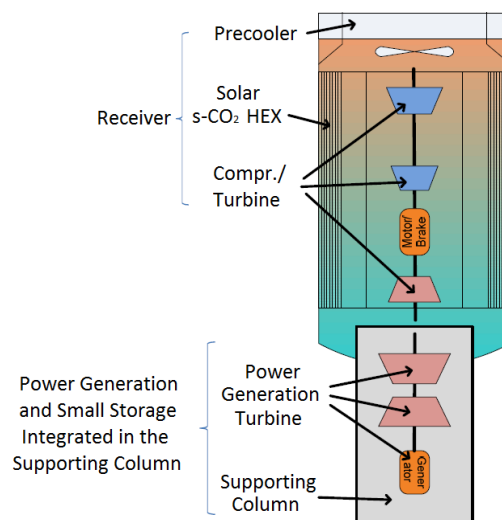


Figure 8. Modular tower receiver with s-CO₂ Brayton cycle [8]

After defining the scenarios for the incorporation of s-CO₂ into CSP plants, recompression and partial cooling cycles were optimised for their conditions (Table 3) and compared. The comparison of the s-CO₂ cycle configurations was performed focusing on the following criteria: cycle efficiency, conductance of recuperators, as a measure of their size, and the temperature increase in the heater, as an indicator of the TES system size.

Table 3. Scenarios conditions

Scenario	Technology	HTF	TES	TIT	Type of Cooling and CIT	Power
1	Parabolic Trough	Thermal Oil	Molten Salts	380°C	Wet (32°C)	50 MW
2	Power Tower	Molten Salts	Molten Salts	550°C	Wet (32°C)	100 MW
3	Modular Tower	s-CO ₂	-	700°C	Wet (32°C)	10 MW
4	Modular Tower	s-CO ₂	-	700°C	Dry (50°C)	10 MW

Other parameters that define the operation of the cycles were assumed to be the same as in previous works [10, 11]:

- Maximum pressure: 25 MPa
- Compressor isentropic efficiency: 89%
- Turbine isentropic efficiency: 93%
- Recuperators effectiveness: 97%
- Minimum temperature difference in heat exchangers: 5°C

2.5 CSP Plant Modelling

After the selection of the s-CO₂ cycle configuration, the complete CSP plant that corresponds to each scenario was modelled in Thermoflex (Appendix D). This was carried out adding the solar field, heat storage and cooling process to the defined s-CO₂ power cycle. In order to obtain more realistic results, some of the assumptions made to model the power cycle were discarded: pressure drops and heat losses are considered in heat exchangers. In addition, from this point on, the net efficiency of the plant was studied instead of the thermal efficiency of the cycle. In this way, mechanical and electrical efficiencies of turbomachinery and auxiliary power are taken into account when evaluating the performance of the plant.

The considerations applied to model the remaining CSP plant parts are described below.

- Since scenarios 1 and 2 represent current CSP technologies, the input data (irradiances, fluids used, time of TES, etc.) correspond to those of the reference plants so that they can be compared.
- In the case of indirect heating of working fluid, the minimum mass flowrate of the HTF is used to achieve the TIT established in the heater and reheater. Moreover, HTF pumps are introduced to propel it throughout the system.
- Thermoflex limits the fluid types that can be used in a solar tower to steam, gas and HTFs. Initially, the s-CO₂ was defined as refrigerant in order to use the database REFPROP. Therefore, to model direct heating of s-CO₂ in a solar tower, the fluid was defined in the towers as a gas, which means utilising an ideal gas model. Given that the conditions are far from the critical point, it can be assumed that its behaviour is close to ideal.
- The direct s-CO₂ heating implies a high-pressure and temperature tower receiver, in which creep effects would be considerable. A study of the pressure drops in a tubular receiver at conditions of scenarios 3 and 4 is presented in Appendix E, based on the analysis of Neises *et al.* [25] and assuming that their results are valid for these conditions.
- Regarding heat storage tanks, the hot salt temperature is set by the HTF temperature coming from the solar field, while the cold salt temperature is constrained by the s-CO₂ inlet temperatures in the heater and reheater.
- The amount of cooling fluid used is also the minimum to reach the CIT in the precooler and intercooler, providing that a pinch point does not occur. Special attention must be paid to precoolers and intercoolers because the operating conditions are close to the critical values.
- The only option in Thermoflex to include dry cooling is using an air-cooled condenser, which is not appropriate since the CO₂ does not change its phase during the cooling process. Hence, the dry cooling is modelled with a heat exchanger and a fan to move the air.

3 RESULTS AND DISCUSSION

In this chapter, the results of this work are shown and discussed. Firstly, the optimisation and comparison of recompression and partial cooling cycles in each scenario are presented. Secondly, the s-CO₂ cycle CSP plants are compared to existing plants to determine the suitability of using a s-CO₂ power cycle.

3.1 Optimisation of Recompression and Partial Cooling Cycles

The maximum efficiency of recompression and partial cooling cycles for the selected scenarios and the values of PR and RPR that maximise this parameter are shown in Table 4. These results were obtained with the EES function 'Min/Max'. As previously mentioned, in order to approve a result, the minimum temperature difference in heat exchangers has to be equal or higher than the one established (5°C) and a pinch point cannot appear in the recuperators.

Table 4. Optimisation results for maximum efficiency

Scenario	Cycle	PR	RPR	η_{th}	Min ΔT_{HX}	Pinch point
1	Recompression	3.19	-	41.42%	3.59°C	LTR
	Partial Cooling	4.17	0.68	39.92%	3.75°C	LTR
2	Recompression	3.27	-	50.26%	7.96°C	LTR
	Partial Cooling	5.03	0.55	49.12%	7.38°C	-
3	Recompression	3.28	-	55.52%	12.14°C	-
	Partial Cooling	5.83	0.46	54.90%	10.77°C	-
4	Recompression	2.59	-	51.33%	12.02°C	-
	Partial Cooling	4.81	0.35	51.39%	11.22°C	-

In the case of scenario 1, neither of the cycles fulfils the minimum temperature difference and pinch point absence. For the recompression cycle in scenario 2, a pinch point takes place in the LTR. Hence, the values of PR and RPR need changing for the maximum efficiency that satisfies the requirements. The following effects are observed when varying separately PR and RPR:

- Increase in PR: the pinch-point problem disappears, however, the minimum temperature difference decreases. Thermal efficiency has a maximum and from this point is reduced, more sharply for recompression cycle.

- Increase in RPR: the pinch-point problem disappears, while the minimum temperature difference increases slightly. In the case of thermal efficiency, it has a maximum value and then is reduced.

The values of PR and RPR are changed accordingly to this analysis and the definitive results for scenario 1 cycles and recompression cycle of scenario 2 can be seen in Table 5. In the first scenario, the minimum temperature difference is lower than 5°C regardless of PR and RPR values. Therefore, a reduction in heat exchanger effectiveness is required, decreasing the thermal efficiency to a greater extent. For recompression cycles, the PR is increased until the pinch point does not occur and regarding partial cooling cycle, the combined effect of PR and RPR results in maximum efficiency when increasing PR and reducing RPR.

Table 5. Optimisation results for scenario 1 and scenario 2 recompression cycle

Scenario	Cycle	PR	RPR	ε	η_{th}	Min ΔT_{HX}
1	Recompression	3.30	-	94.5%	40.17%	5.17°C
	Partial Cooling	4.65	0.63	95%	39.06%	5.14°C
2	Recompression	3.29	-	97%	50.22%	7.77°C

The results show that the smaller the difference between the highest and lowest temperatures of the cycle, the more complicated it is to optimise the cycle. The conditions at which scenario 1 cycles satisfy the requirements are far from the maximum efficiency point, in contrast to scenario 2 where the recompression cycle only increased slightly its PR. The other scenarios results for maximum efficiency are acceptable, having higher temperature difference throughout the cycle. In addition, for scenario 1 cycles, the minimum temperature difference cannot be managed unless the effectiveness of the recuperators is reduced. The reason behind this is that the same minimum temperature difference is established for all the scenarios regardless of their temperature conditions.

Comparing the optimisation of the two cycles, the recompression cycle presents a greater tendency to have a pinch point and reduces its thermal efficiency to a higher extent than the partial cooling cycle in order to solve this problem. In addition, the partial cooling cycle efficiency is less sensitive to PR, remaining more constant when this parameter varies from the maximum efficiency point.

3.2 Comparison of Recompression and Partial Cooling Cycles

The recompression and partial cooling cycles are compared for each scenario in order to determine the most appropriate s-CO₂ cycle configuration to implement into the corresponding CSP plant. In Table 6, the results that are significant for the comparison are shown: thermal efficiency, total conductance of recuperators and temperature increase in the heater. It must be taken into account that these results are limited to the assumptions taken during the modelling process, such as the absence of pressure drops and heat losses in heat exchangers, which would affect the three parameters compared.

Table 6. Comparison of recompression and partial cooling cycles results

Scenario	Cycle	η_{th}	UA	ΔT_{Heater}
1	Recompression	40.17%	14.56 MW/K	104°C
	Partial Cooling	39.06%	9.55 MW/K	139°C
2	Recompression	50.22%	21.86 MW/K	133°C
	Partial Cooling	49.12%	13.68 MW/K	180°C
3	Recompression	55.52%	1.58 MW/K	153°C
	Partial Cooling	54.90%	0.96 MW/K	217°C
4	Recompression	51.33%	2.23 MW/K	121°C
	Partial Cooling	51.39%	1.11 MW/K	195°C

The results are discussed below, analysing individually each comparison factor.

- **Thermal efficiency:** this parameter is slightly higher for the recompression cycle in scenarios 1 to 3. However, when introducing dry cooling in scenario 4, the situation is reversed. Taking scenario 3 results as a reference, the partial cooling cycle undergoes a smaller efficiency reduction than the recompression cycle. Although the partial cooling cycle narrowly exceeds recompression efficiency, it is a meaningful result for CSP application.
- **Conductance of recuperators:** s-CO₂ cycle costs are greatly determined by the size of the recuperators, which can be measured roughly with their conductance [11]. This criterion is in favour of the partial cooling cycle in all the scenarios, since its conductance is 1.5-2 times smaller than in recompression cycle. To compare the conductance results among scenarios, it must be taken into account that the conductance values are dependent on the power output.

- **Temperature increase in the heater:** the temperature difference of the HTF leaving and returning to the solar field impacts directly on the TES system size because the amount of storage medium is inversely proportional to it. The temperature change of the HTF is mainly determined by the s-CO₂ temperature increase in the heater and this last parameter can indicate approximately the energy storage size [11]. Again, partial cooling cycle benefits in all the scenarios in comparison with recompression cycle. Another advantage drawn from these data is that the maximum temperature achieved in the HTR is lower for partial cooling, which can reduce material issues.

In view of the results obtained, the partial cooling cycle is certainly the best configuration at the conditions of the fourth scenario given that it overcomes the recompression cycle in the three aspects studied. Regarding the other scenarios, the partial cooling cycle presents slightly lower thermal efficiency but benefits related to a reduction of costs: smaller recuperators, fewer materials issues in the HTR and reduced TES system. This is in line with Turchi and Neises results [11], which correspond to operating conditions close to the scenario 4. With the present work, it is confirmed that the partial cooling advantages remain for wider operating conditions. Moreover, it is noticed that, as the scenarios progress and TIT is higher, partial cooling advantages over recompression are greater and the efficiency difference between the cycles is reduced until being surpassed in scenario 4.

A suitable way to determine the most appropriate cycle would be an economic evaluation, determining if the smaller efficiency of the partial cooling cycle can be compensated with lower costs in key elements of the plant (recuperators and TES). Unfortunately, the early stage of development in s-CO₂ cycle technology and the lack of available information hampers an economic study. Consequently, the selection of the s-CO₂ cycle layout is done qualitatively.

Abengoa Solar compared partial cooling and recompression cycles for tower technology and molten salts heat storage, which resulted in a 3% lower levelised cost of electricity of the former cycle [26]. Assuming that this study corresponds to the scenario 2, the partial cooling cycle is chosen in this case. The results of

scenario 1 are proportionally similar to those of scenario 2, hence the same cycle is selected. Finally, scenario 3 does not include heat storage and the advantages of partial cooling cycle are decreased. Nevertheless, this cycle is also chosen because the efficiency difference with the recompression cycle is smaller than in previous scenarios and it serves as a reference for scenario 4, where the only change is the introduction of dry cooling.

3.3 Comparison of S-CO₂ Cycle CSP Plants with Current Plants

Since the s-CO₂ cycle is considered an alternative to steam Rankine cycle, it is essential to compare the performance of s-CO₂ cycle CSP plants with that of existing plants, represented by the reference plants. The following characteristics are studied: the net efficiency of the CSP plant in the design point, the cooling fluid flowrate and the TES system size.

3.3.1 Net Plant Efficiency

The net efficiencies of the s-CO₂ cycle CSP plants corresponding to the four scenarios are shown in Figure 9, where they can be compared to those of current Rankine cycle CSP plants.

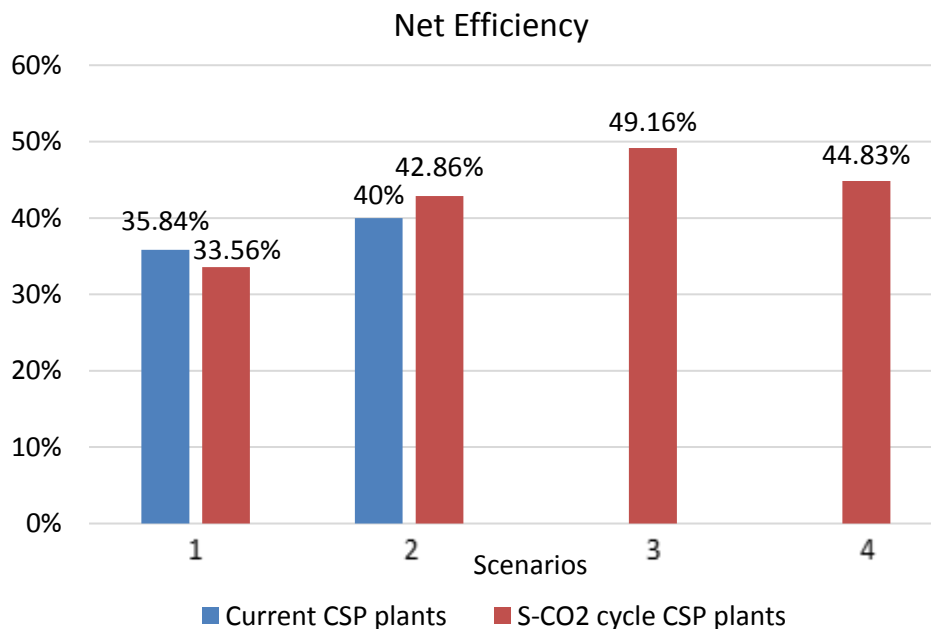


Figure 9. Net efficiency of current and s-CO₂ cycle CSP plants

According to the results, the parabolic trough (scenario 1) is the only technology that cannot improve the efficiency of existing CSP plants with s-CO₂ partial cooling cycle. The reasons behind this are the temperature limitation set by the thermal oil used as HTF (TIT=380°C) and the reduction of heat exchanger effectiveness during the optimisation process. The resulting lower efficiency is in concordance with the fact that the s-CO₂ cycle is considered an alternative to the steam Rankine cycle for TIT higher than 500°C [1].

In fact, the use of molten salts as the HTF or direct heating allows s-CO₂ cycle CSP plants to exceed existing plants efficiency due to the higher operating temperatures. When molten salts are used in a central tower (scenario 2), the net efficiency of the s-CO₂ cycle CSP plant increases by more than 9% points in comparison with parabolic trough, overcoming the reference tower plant.

Concerning direct heating scenarios, they have even a greater performance than scenario 2 plant. The highest plant efficiency corresponds to direct heating with wet cooling (49.16%), which is reduced 4.3% points when using dry cooling. It must be taken into consideration that the pressure drops resulting from the receiver analysis (Appendix E) were not introduced in Thermoflex because they were too large (30-40%). Instead, it was assumed that this receiver design would not be used in an actual CSP plant but other one that would produce smaller pressure drops (0.5%). Therefore, the net efficiency results of scenarios 3 and 4 are constrained by this assumption.

3.3.2 Cooling Fluid Flowrate

Initially, the cooling fluid flowrate used in the coolers was determined as the minimum that was required to reach the CIT, undergoing a maximum temperature increase. However, when performing simulations with these data in Thermoflex for the wet cooling scenarios (1 to 3), it was not possible to achieve the target temperature in the intercooler. In the partial cooling cycles of these scenarios, the CO₂ passing through the intercooler is at conditions close to the critical point. The sharp change of properties, particularly of the specific heat, produces the following temperature profile in the intercooler (Figure 10). The profile shown

corresponds to the second scenario, where the occurrence of a pinch point is noticeable and the temperature of 32°C is not reached.

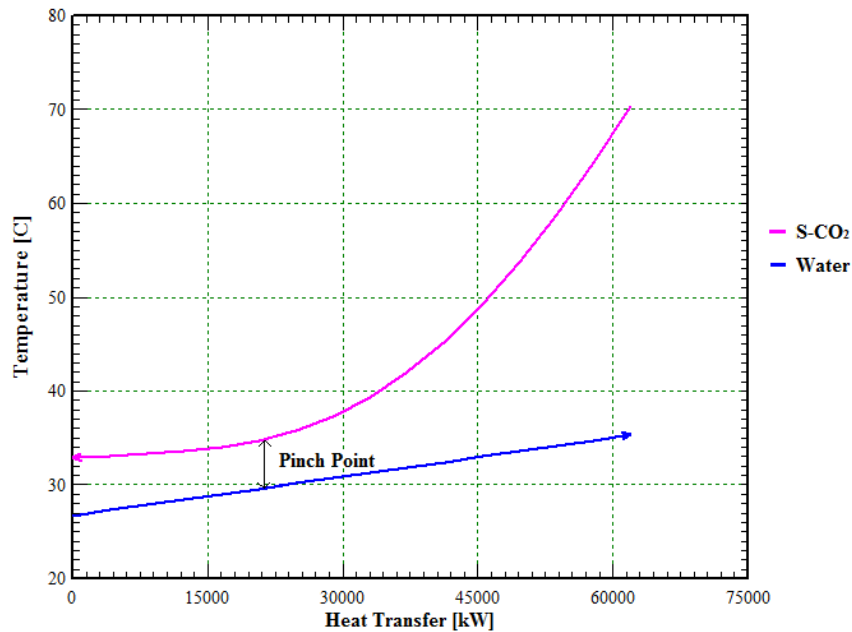


Figure 10. Temperature profile in the intercooler of scenario 2 for the minimum cooling water flowrate

In order to solve this pinch-point problem, the mass flowrate of the water going to the intercooler is increased to match the heat capacities of both fluids, until a pinch point does not happen. On the contrary, the amount of water sent to the precooler can be decreased to minimise the total water flowrate. In the case of dry cooling, there is not any pinch-point problem and the minimum flowrate works. In Table 7, the required cooling fluid flowrates are presented.

Table 7. Cooling fluid flowrates

Scenario	Intercooler	Precooler	Total
1	7,000 kg/s	500 kg/s	7,500 kg/s
2	5,500 kg/s	500 kg/s	6,000 kg/s
3	500 kg/s	50 kg/s	550 kg/s
4	401 kg/s	299 kg/s	700 kg/s

As it can be appreciated, in scenarios 1 to 3 the intercooler is what mainly determines the water flowrate needed, while in scenario 4 the flowrates are divided proportionally to the heat rejected.

The comparison of the different scenarios can be performed considering the total cooling fluid flowrate per MW of electricity produced (Figure 11).

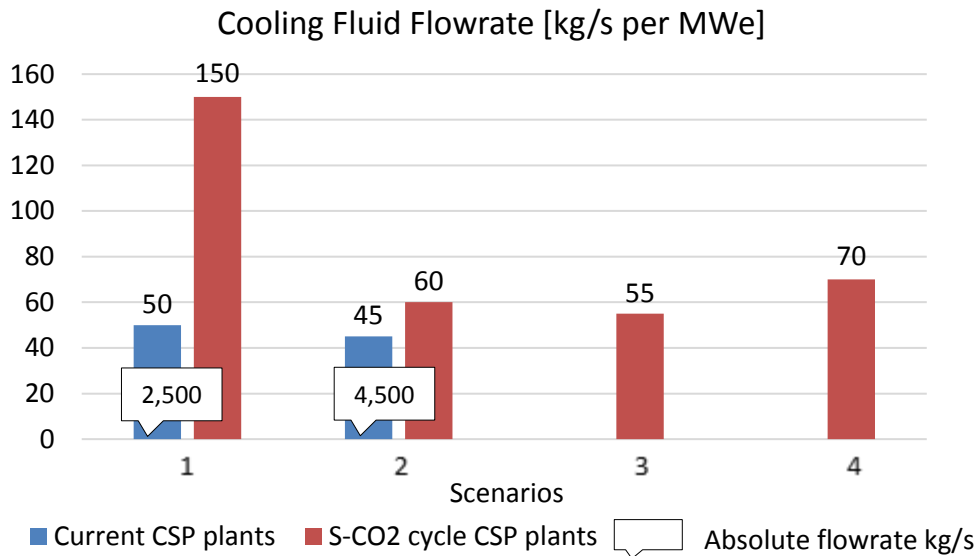


Figure 11. Comparison of cooling fluid flowrate of current and s-CO₂ cycle CSP plants

The s-CO₂ cycle CSP plants with wet cooling require even higher amount of water than current plants, especially in the case of parabolic trough technology. On the other hand, the air flowrate of scenario 4 can seem high in comparison with current plants water flowrate. However, taking into account that the specific heat of air is four times smaller than that of water, the air flowrate is proportionally reduced due to the higher plant efficiency.

3.3.3 Thermal Energy Storage System Size

The size of the TES system is presented in Table 8 for current and s-CO₂ cycle CSP plants in scenarios 1 and 2. Since the two scenarios use molten salts stored in two tanks, the volume of one of the tanks is given. Despite the fact that the hot salt tank is slightly bigger, it can be considered that the two tanks have the same dimensions (Thermoflex makes this assumption).

Table 8. Tanks volume of current and s-CO₂ cycle CSP plants

Scenario	Current CSP Plants	S-CO ₂ Cycle CSP Plants
1	14,250 m ³	13,766 m ³
2	27,280 m ³	35,086 m ³

The results of the tanks volume show that a parabolic trough CSP plant (scenario 1) with s-CO₂ partial cooling cycle has smaller salt tanks than a current plant of this type. In both plants, the temperature of the hot salts is 386°C since it is set by the temperature of the thermal oil coming from the solar field. The cold salts temperature is 292°C in current plants, while in s-CO₂ cycle plants this temperature is reduced until 286°C. The higher temperature difference of s-CO₂ cycle CSP plants allows them to have smaller TES tanks.

However, in the case of central tower technology (scenario 2), the situation is reversed. Having the same hot salts temperature (565°C), current plants present a temperature of 290°C for the cold salts and s-CO₂ cycle plants, 429.4°C. The reduction of the temperature difference when using a s-CO₂ power cycle is considerable, and thus, the increase in the volume of the heat storage tanks as well.

4 CONCLUSIONS AND RECOMMENDATIONS

Although the benefits of the s-CO₂ power cycle have been known for decades, its application is quite novel and is still in a demonstration stage. Many studies have been carried out for different applications and the use of a s-CO₂ cycle could be a way of making future CSP plants more efficient and cheaper. The purpose of this project was to study the suitability of integrating s-CO₂ cycle into CSP applications, therefore the comparison with current plants was essential.

The following conclusions were drawn from this work:

- A s-CO₂ cycle based on partial cooling layout has advantages for CSP plants over recompression cycle in the four scenarios: lower costs of recuperators and TES system, less material issues in the HTR and less efficiency reduction when dry cooling is used. However, these benefits must be confirmed with an economic study performed specifically for these scenarios.
- The use of wet cooling results contradictory when it is used with s-CO₂ power cycle. It allows CSP plants to have a low temperature of heat rejection and maximise their efficiency but, regardless of the scenario, a high flowrate of cooling water is demanded to avoid a pinch point in the intercooler. This result is totally opposed to the requirement of water consumption minimisation since CSP plants are normally placed in arid regions.
- The utilisation of s-CO₂ power cycle in a parabolic trough CSP plant presents drawbacks since the beginning of the analysis, such as the reduction of the cycle efficiency to avoid a pinch point in the LTR and to have an acceptable temperature difference in heat exchangers. In view of its results, this scenario can be finally discarded as a viable option to incorporate s-CO₂ power cycle due to its low net efficiency and remarkably high amount of cooling water required in comparison with current plants.
- The s-CO₂ power cycle could be incorporated into a central tower CSP plant type with molten salts since this plant would have a better efficiency than current plants and the technology is already mature and available. However, it presents important disadvantages: a higher cooling water flowrate and bigger

tanks to store the salts than current plants. This might reject the deployment of s-CO₂ cycle in this scenario if the higher efficiency cannot compensate the higher costs associated with the cooling and TES processes. The use of dry cooling was not studied for this type of plant, but it would presumably reduce the net efficiency 4% points, to a value lower than that of existing plants. In any case, the suitability of introducing a s-CO₂ cycle in a central tower plant with wet or dry cooling must be determined economically and by comparison with current plants.

- The option of direct heating of s-CO₂ in CSP plants shows a possible implementation for both wet and dry cooling, considering the results obtained. In the case of wet cooling, despite the fact that it would require a higher amount of cooling water than existing plants, this could be acceptable since the net efficiency of the plant would greatly increase. Regarding dry cooling, the cooling process would be more affordable and the plant efficiency still quite high. However, this type of CSP technology requires the development of a high-pressure s-CO₂ receiver and a TES system for high temperature, which probably will not happen until the commercial viability of the s-CO₂ power cycle itself is demonstrated.

Among the scenarios considered, the greatest potential is shown by a high temperature CSP plant that would employ direct heating of s-CO₂, a partial cooling configuration and dry cooling, resulting in a net plant efficiency up to nearly 45%. This value is considerably higher than existing CSP plants and comparable to that of an ultra-supercritical Rankine cycle plant, used for fossil fuel application with wet cooling [27]. Therefore, the key benefit of this CSP plant is that it could reach such a high plant efficiency with dry cooling, reducing to a great extent the water consumption of the plant and its associated costs.

Further work is required to be done in the analysis of the implementation of s-CO₂ cycle into CSP plants. Although the demonstration stage of this technology makes it difficult to perform economic evaluations, a more precise model of the s-CO₂ power cycle could help in this aspect, especially in the case of the recuperators because they represent an important cost of this cycle. Therefore,

future work could include calculations of heat transfer coefficients, pressure drops and actual dimensions of the recuperators. The wet cooling process, modelled in this work with Thermoflex, could be introduced in the models of s-CO₂ power cycles created in EES in order to study more deeply the occurrence of a pinch point in the coolers. It has been demonstrated that this problem has a great impact on the amount of cooling water required.

In the present work, only two configurations of the s-CO₂ power cycle were considered because they present high efficiency, while being simple. However, more complex layouts could have higher efficiencies and benefits for CSP application, such as the addition of a bottom cycle. Regarding the simulations of CSP plants, they were performed for the design point of the plant. Moreover, it is necessary to study the s-CO₂ cycle at off-design conditions and carry out daily and yearly simulations to fully understand the behaviour of a CSP plant that uses a s-CO₂ power cycle.

REFERENCES

- [1] Ahn, Y., Bae, S.J., Kim, M., Cho, S.K., Baik, S., Lee, J.I. and Cha, J.E. (2015), 'Review of Supercritical CO₂ Power Cycle Technology and Current Status of Research and Development', *Nuclear Engineering and Technology*, 47(6), pp. 647-661.
- [2] Feher, E.G. (1967), 'The Supercritical Thermodynamic Power Cycle', *Proceedings of the IECEC*, Miami Beach, Florida, 13-17 August 1967.
- [3] Angelino, G. (1968), 'Carbon Dioxide Condensation Cycles for Power Production', *J. Eng. Power*, 90(3), pp. 287-295.
- [4] Wright, S.A., Radel R.F., Vernon, M.E., Rochau, G.E. and Pickard, P.S. (2010), *Operation and Analysis of a Supercritical CO₂ Brayton Cycle*, SAND2010-0171.
- [5] Echogen Power Systems (2016), *Echogen: Our Solution*. Available at: <http://www.echogen.com/our-solution/> (Accessed: 25 July 2016)
- [6] Dostal, V., Driscoll, M.J. and Hejzlar, P. (2004), *MIT-ANP-TR-100: A Supercritical Carbon Dioxide Cycle for Next Generation Nuclear Reactors*, Massachusetts Institute of Technology.
- [7] Moisseytsev, A. and Sienicki, J.J. (2009), 'Investigation of Alternative Layouts for the Supercritical Carbon Dioxide Brayton Cycle for a Sodium-cooled Fast Reactor', *Nuclear Engineering and Design*, 239(7), pp. 1362-1371.
- [8] Turchi, C.S. and Ma, Z. (2011), 'Advanced Supercritical Carbon Dioxide Power Cycle Configurations for Use in Concentrating Solar Power Systems', *Proceedings of Supercritical CO₂ Power Cycle Symposium*, Boulder, Colorado, 24-25 May 2011.
- [9] Turchi, C.S., Ma, Z. and Dyreby, J. (2012), 'Supercritical Carbon Dioxide Power Cycle Configurations for Use in Concentrating Solar Power Systems', *Proceedings of ASME Turbo Expo 2012*, Copenhagen, Denmark, 11-15 June 2012.

- [10] Turchi, C.S., Ma, Z., Neises, T.W. and Wagner, M.J. (2013), 'Thermodynamic Study of Advanced Supercritical Carbon Dioxide Power Cycles for Concentrating Solar Power Systems', *Journal of Solar Energy Engineering*, 135(4), pp. 041007-041007-7.
- [11] Turchi, C.S. and Neises, T.W. (2014), 'Supercritical CO₂ Power Cycles: Design Considerations for Concentrating Solar Power', *Proceedings of Supercritical CO₂ Power Cycle Symposium*, Pittsburgh, Pennsylvania, 9-10 September 2014.
- [12] Besarati, S.M. and Goswami D.Y. (2013), 'Analysis of Advanced Supercritical Carbon Dioxide Power Cycles with a Bottoming Cycle for Concentrating Solar Power Applications', *Journal of Solar Energy Engineering*, 136(1), pp. 010904-010904-7.
- [13] Seidel, W. (2010), *Model Development and Annual Simulation of the Supercritical Carbon Dioxide Brayton Cycle for Concentrating Solar Power Applications*, MSc Thesis, University of Wisconsin-Madison.
- [14] Dostal, V. and Kulhánek, M. (2011), 'Thermodynamic Analysis and Comparison of Supercritical Carbon Dioxide Cycles', *Proceedings of Supercritical CO₂ Power Cycle Symposium*, Boulder, Colorado, 24-25 May 2011.
- [15] Kelly, B. (2010), *Advanced Thermal Storage for Central Receivers with Supercritical Coolants, Final Report under Grant DE-FG36-08G018149*, Abengoa Solar Inc., Lakewood, Colorado.
- [16] National Institute of Standards and Technology (2013), *NIST Reference Fluid Thermodynamic and Transport Properties—REFPROP. Version 9.1. User's Guide*.
- [17] Nellis, G. and Klein, S. (2009), *Heat Transfer*, Cambridge University Press.
- [18] Thermoflow, Inc. (2015), *Thermoflex. Fully-Flexible Heat Balance Engineering Software*.

- [19] Chaanaoui, M., Vaudreuil, S. and Bounahmidi, T. (2016), 'Benchmark of Concentrating Solar Power Plants: Historical, Current and Future Technical and Economic Development', *Procedia Computer Science*, 83(2016), pp. 782-789.
- [20] NREL (2015), *Concentrating Solar Power Projects*. Available at: <http://www.nrel.gov/csp/solarpaces/index.cfm> (Accessed: 20 July 2016)
- [21] Ramos Quesada, P. (2016), *A Global CSP (Concentrated Solar Power) Model Development*, MSc Thesis, Cranfield University.
- [22] U.S. Department of Energy (2014), *2014: The Year of Concentrating Solar Power*, DOE/EE-110.
- [23] Novotec (2007), *Estudio de Impacto Ambiental: Planta de Generación Solar Termoeléctrica de 17 MWe en Finca la Monclova y Línea de Evacuación hasta Subestación Villanueva del Rey (Sevilla)*, Report 07/372/51006 (in Spanish).
- [24] Adame Barrera, J. (2015), *Diseño y Análisis del Comportamiento de un Aerocondensador en una Central Termosolar*, Final Degree Project, University of Seville (in Spanish).
- [25] Neises, T.W., Wagner, M.J. and Gray, A.K. (2014), 'Structural Design Considerations for Tubular Power Tower Receivers Operating at 650°C', *Proceedings of the 8th International Conference on Energy Sustainability*, Boston, Massachusetts, 30 June-2 July 2014.
- [26] Turchi, C.S. (2014), *10 MW Supercritical CO₂ Turbine Test*, DE-EE0001589, NREL.
- [27] IEA (2012), *Technology Roadmap: High-Efficiency, Low-Emissions Coal-Fired Power Generation*, OECD/IEA.

APPENDICES

Appendix A S-CO₂ Power Cycle Layouts

This appendix includes a review of the main s-CO₂ power cycles [4]. The basic cycle is the simple recuperated Brayton cycle, which is modified to obtain the rest of the cycle layouts. This variations pursue an increase in cycle efficiency. They cover stages of reheating and intercooling, and the compound cycles proposed by Angelino [3] with the aim of avoiding the pinch-point problem.

A.1 Simple Recuperated Brayton Cycle

This cycle is the most simple and requires the lowest number of components, as it can be seen in Figure A-1.

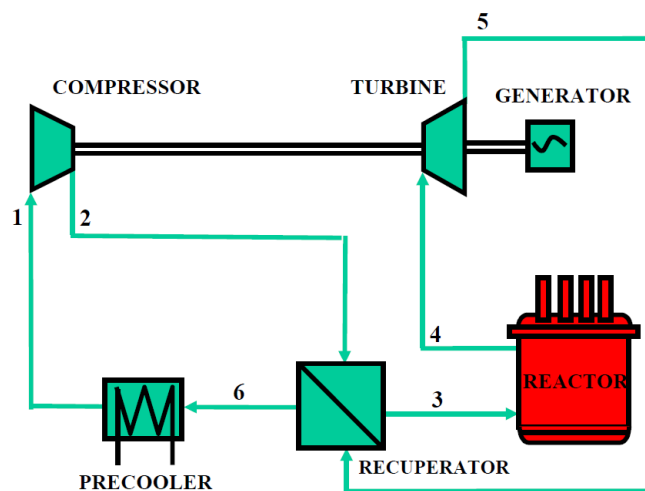


Figure A-1. Simple recuperated Brayton Cycle [4]

The s-CO₂ exits the compressor at high pressure and is preheated in the recuperator by the hot stream leaving the turbine. Then, it is heated by the energy source and expands in the turbine. Finally, after transferring heat in the recuperator, the fluid is cooled in the pre-cooler until reaching the compressor inlet conditions. The process of heat recuperation is required to achieve high thermal efficiency because the turbine outlet temperature is high.

A.2 Reheated Brayton Cycle

The cycle shown in Figure A-2 corresponds to a single stage of reheating. In this case, the expansion of the s-CO₂ is divided into two so that the fluid can be heated again before the low pressure turbine. The optimum pressure ratio split in the reheating stage is close to equal due to the similar behaviour of s-CO₂ to ideal gas in the expansion region.

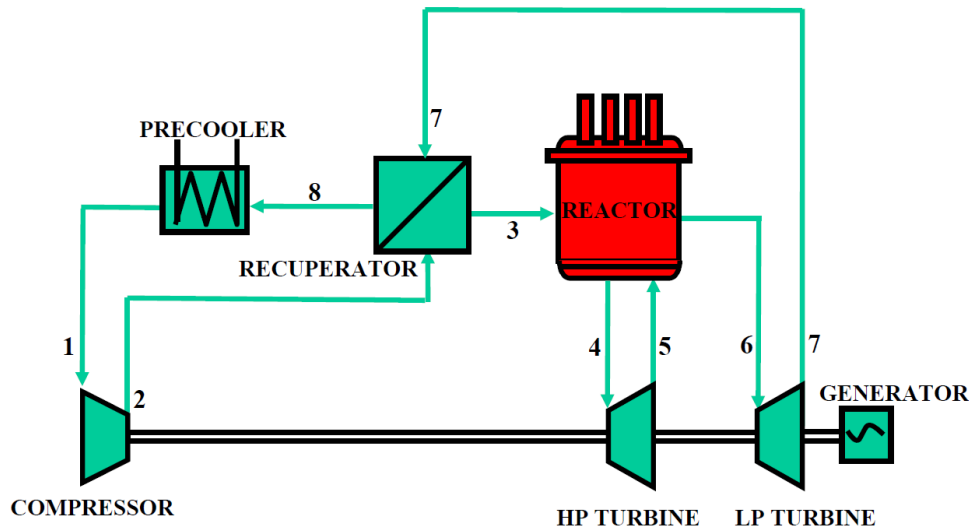


Figure A-2. Reheated Brayton cycle [4]

This layout improves the cycle efficiency by increasing the average temperature of heat addition. However, the pressure drop in the reheater may offset the benefit of reheating and as a consequence, more than one stage of reheating is not recommended.

A.3 Intercooled Brayton Cycle

In this cycle, a stage of intercooling is introduced in the compression process (Figure A-3). For ideal gas cycles, the compression work is noticeably reduced due to compressing the fluid at lower temperatures. For a s-CO₂ power cycle, this improvement is smaller since the compression process is performed close to the critical point and it is already low. In addition, the pressure ratio split is not equal because of the real gas behaviour and has to be optimised.

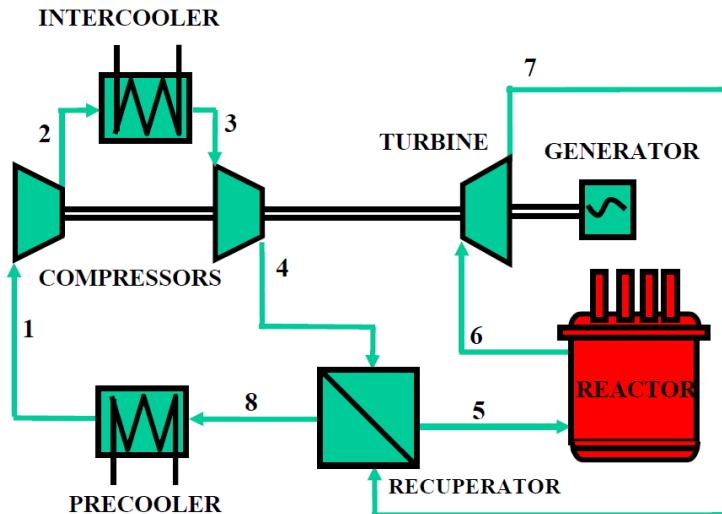


Figure A-3. Intercooled Brayton cycle [4]

The benefit in cycle efficiency comes from reducing the average temperature of heat rejection. However, the small improvement is not worth the complication of the system.

A.4 Compound Brayton Cycles

Angelino [3] introduced the compound cycles in order to prevent the pinch-point problem and reduce the irreversibilities in the recuperator. Those cycles use precompression or recompression, resulting in higher efficiency but more complex layouts: the recuperator is split into two and more components are required.

A.4.1 Precompression Cycle

The precompression cycle, shown in Figure A-4, divides the recuperator into two so that the hot s-CO₂ downstream the turbine is compressed between the two recuperators. The hot side stream in the recuperators has low specific heat. In order to avoid the temperature difference to become too small in the low temperature recuperator (LTR), the precompression compressor (PC) increases the specific heat of the hot stream by a pressure rise. As a result, more heat is available to be regenerated and the cycle efficiency is increased in comparison with the simple Brayton cycle.

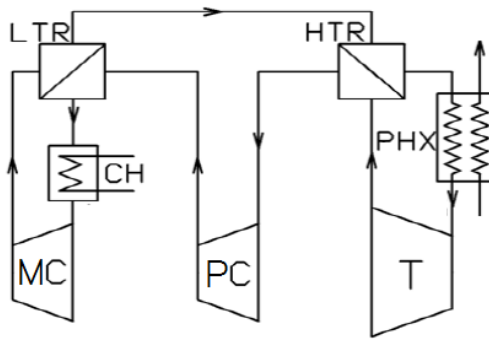


Figure A-4. Precompression cycle [7]

A.4.2 Recompression Cycle

In the recompression cycle (Figure A-5), the hot fluid passes through both recuperators after leaving the turbine. Unlike precompression cycle, the flow is split before the pre-cooler: one part is cooled in the pre-cooler, compressed and preheated in the LTR, while the other part is only compressed. The two streams are merged before the high temperature recuperator (HTR). The effect of the flow division is that the specific heat difference between the streams is compensated with different mass flowrates and the heat capacities are equalised in the LTR. Since the hot side stream has low specific heat, the mass flowrate of the cold stream is reduced.

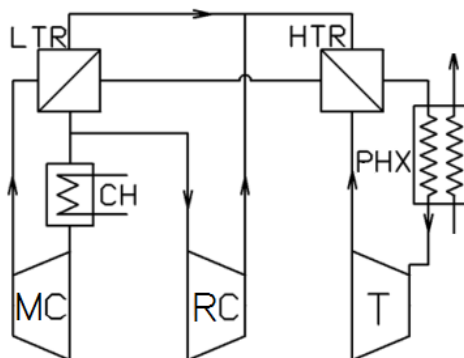


Figure A-5. Recompression cycle [7]

This configuration, in addition to prevent the pinch-point problem, also increases the cycle efficiency by reducing the heat rejection from the cycle because only a fraction of the fluid does it. It is generally considered the most efficient s-CO₂ power cycle.

A.4.3 Partial Cooling Cycle

The partial cooling cycle, shown in Figure A-6, results from the combination of precompression and recompression cycles. In this case, the precompression compressor is situated after the LTR together with an additional precooler. These components are followed by the flow split, characteristic of recompression cycle.

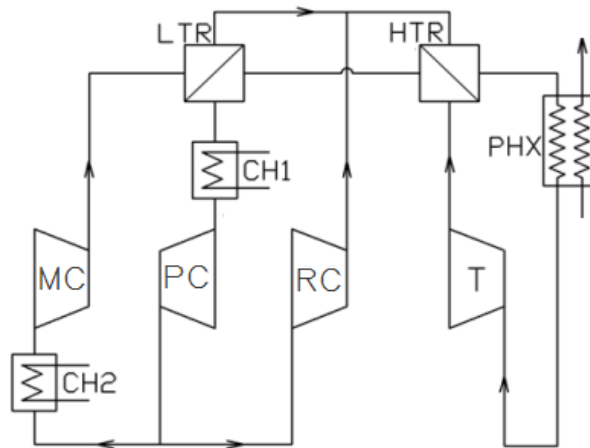


Figure A-6. Partial cooling cycle [7]

In spite of combining features of two previous cycles, the efficiency of the partial cooling cycle is similar to that of the recompression cycle. Since partial cooling cycle has two more components, recompression cycle is commonly preferred.

Appendix B Discretisation of Heat Exchangers

In this appendix the methodology used to discretise the heat exchangers is presented. It was developed according to Nellis and Klein [13] and consists in dividing the heat exchanger into N sub-heat exchangers (Figure A-7), so that the changes in s-CO₂ properties are considered.

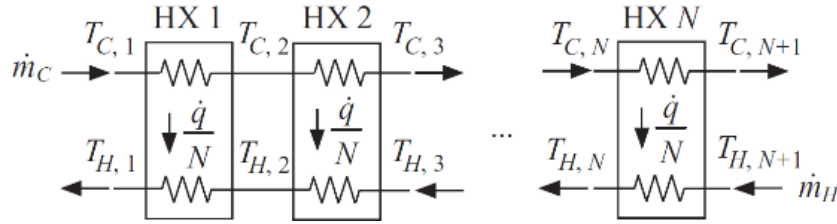


Figure A-7. Discretisation of a counter-flow heat exchanger into sub-heat exchangers

Since the effectiveness model is first used, the properties (temperature, pressure, enthalpy and mass flowrate) of the inlet and outlet streams of the heat exchanger are defined. Therefore, the total heat transfer rate of the heat exchanger can be calculated:

$$\dot{Q} = \dot{m}_H(h_{H,in} - h_{H,out}) = \dot{m}_C(h_{C,out} - h_{C,in}) \quad (\text{A-1})$$

The division of the heat exchanger into N sub-heat exchangers implies that they exchange an equal heat transfer rate \dot{Q}/N .

The two streams used to start obtaining the temperature profile of the heat exchanger sides are the cold-side inlet and the hot-side outlet streams. Carrying out subsequent energy balances on the hot and cold sides of each sub-heat exchanger, the enthalpies of the cold-side outlet and hot-side inlet streams are determined.

$$h_{H,i+1} = h_{H,i} + \frac{\dot{Q}}{\dot{m}_H N}; i = 1..N \quad (\text{A-2})$$

$$h_{C,i+1} = h_{C,i} + \frac{\dot{Q}}{\dot{m}_C N}; i = 1..N \quad (\text{A-3})$$

Once the enthalpies are known, the temperature distribution in the heat exchanger is obtained with the data of pressure.

Regarding the determination of sub-heat exchangers conductances, the ε -NTU solution is individually applied. Firstly, the heat capacities of the hot and cold streams in each sub-heat exchanger are computed. Despite the fact that s-CO₂ specific heat varies along the heat exchanger, it can be assumed that it is constant in each sub-heat exchanger due to the discretisation of the temperature profiles. The constant specific heat of the hot and cold streams in each sub-heat exchanger is an average value, defined as the difference of enthalpies divided by the difference of temperatures experienced by that stream.

$$\dot{C}_{H,i} = \dot{m}_H c_{H,i} = \dot{m}_H \frac{(h_{H,i+1} - h_{H,i})}{(T_{H,i+1} - T_{H,i})} ; i = 1..N \quad (\text{A-4})$$

$$\dot{C}_{C,i} = \dot{m}_C c_{C,i} = \dot{m}_C \frac{(h_{C,i+1} - h_{C,i})}{(T_{C,i+1} - T_{C,i})} ; i = 1..N \quad (\text{A-5})$$

The effectiveness of each sub-heat exchanger is then calculated: the actual heat transfer rate is \dot{Q}/N and the maximum heat transfer rate is the product of the minimum heat capacity and maximum temperature difference.

$$\varepsilon_i = \frac{\dot{Q}/N}{\min(\dot{C}_{H,i}, \dot{C}_{C,i}) (T_{H,i+1} - T_{C,i})} ; i = 1..N \quad (\text{A-6})$$

The conductance required in each sub-heat exchanger is determined by the number of transfer units (NTU), which is obtained with the standard ε -NTU solution for a counter-flow heat exchanger.

$$UA_i = NTU_i \min(\dot{C}_{H,i}, \dot{C}_{C,i}) ; i = 1..N \quad (\text{A-7})$$

Finally, the overall conductance of the heat exchanger results from the addition of the individual conductances of the sub-heat exchangers:

$$UA = \sum_{i=1}^N UA_i \quad (\text{A-8})$$

Appendix C Code Implemented in EES

This appendix contains the code developed in the software EES to model the recompression and partial cooling cycles. The code also includes the heat exchangers discretisation explained in the previous appendix. The input data section must be completed with the operating conditions that are simulated..

C.1 Recompression Cycle EES Code

{UNITS: Pressure (MPa), Temperature (°C), Mass (kg), Energy (kJ)}

{INPUT DATA}

```
CIT= {°C}
TIT= {°C}
P_max= {MPa}
PR= {-}
eta_C= {-}
eta_T= {-}
epsilon_HTR= {-}
epsilon_hot= {-}
W_net= {kW}
N= {-}
```

{THERMODYNAMIC CYCLE}

```
P_min=P_max/PR
P_int=(P_max+P_min)/2

T_1=TIT
P_1=P_max
h_1=Enthalpy(CarbonDioxide;T=T_1;P=P_1)
s_1=Entropy(CarbonDioxide;T=T_1;P=P_1)

P_2s=P_int
s_2s=s_1
h_2s=Enthalpy(CarbonDioxide;P=P_2s;s=s_2s)

eta_T=(h_1-h_2)/(h_1-h_2s)
P_2=P_int
T_2=Temperature(CarbonDioxide;P=P_2;h=h_2)

T_3=TIT
P_3=P_int
h_3=Enthalpy(CarbonDioxide;T=T_3;P=P_3)
s_3=Entropy(CarbonDioxide;T=T_3;P=P_3)

P_4s=P_min
s_4s=s_3
h_4s=Enthalpy(CarbonDioxide;P=P_4s;s=s_4s)

eta_T=(h_3-h_4)/(h_3-h_4s)
P_4=P_min
T_4=Temperature(CarbonDioxide;P=P_4;h=h_4)

T_7=CIT
P_7=P_min
h_7=Enthalpy(CarbonDioxide;T=T_7;P=P_7)
s_7=Entropy(CarbonDioxide;T=T_7;P=P_7)
```

P_8s=P_max
s_8s=s_7
h_8s=Enthalpy(CarbonDioxide;P=P_8s;s=s_8s)

eta_C=(h_8s-h_7)/(h_8-h_7)
P_8=P_max
T_8=Temperature(CarbonDioxide;P=P_8;h=h_8)

P_6=P_min
epsilon_hot=(h_4-h_6)/(h_4-Enthalpy(CarbonDioxide;T=T_8;P=P_6))
T_6=Temperature(CarbonDioxide;P=P_6;h=h_6)
s_6=Entropy(CarbonDioxide;P=P_6;h=h_6)

P_10s=P_max
s_10s=s_6
h_10s=Enthalpy(CarbonDioxide;P=P_10s;s=s_10s)

P_10=P_max
eta_C=(h_10s-h_6)/(h_10-h_6)
T_10=Temperature(CarbonDioxide;P=P_10;h=h_10)

T_9=T_10
P_9=P_10
h_9=h_10

T_11=T_10
P_11=P_10
h_11=h_10

P_5=P_min
epsilon_HTR=(h_4-h_5)/(h_4-Enthalpy(CarbonDioxide;T=T_11;P=P_5))
T_5=Temperature(CarbonDioxide;P=P_5;h=h_5)

h_12-h_11=h_4-h_5
P_12=P_max
T_12=Temperature(CarbonDioxide;P=P_12;h=h_12)

{CYCLE PERFORMANCE}

SR*(h_9-h_8)=h_5-h_6

W_HPT=m*(h_1-h_2)
W_LPT=m*(h_3-h_4)
W_MC=SR*m*(h_8-h_7)
W_RC=(1-SR)*m*(h_10-h_6)
W_net=W_HPT+W_LPT-W_MC-W_RC

Q_heat=m*(h_1-h_12)
Q_reheat=m*(h_3-h_2)
Q_in=Q_heat+Q_reheat

eta_th=W_net/Q_in*100

epsilon_LTR=(h_5-h_6)/(h_5-Enthalpy(CarbonDioxide;T=T_8;P=P_6))

{HTR}

T_Cin_HTR=T_11
T_Cout_HTR=T_12
T_Hin_HTR=T_4
T_Hout_HTR=T_5
P_C_HTR=P_max
P_H_HTR=P_min
h_Cin_HTR=h_11
h_Cout_HTR=h_12
h_Hin_HTR=h_4

```

h_Hout_HTR=h_5

Q_HTR=m*(h_Hin_HTR-h_Hout_HTR)
Q_HTR2=m*(h_Cout_HTR-h_Cin_HTR)
T_H_HTR[1]=T_Hout_HTR
T_C_HTR[1]=T_Cin_HTR
h_H_HTR[1]=h_Hout_HTR
h_C_HTR[1]=h_Cin_HTR

Duplicate i=1;N
  Q_HTR[i]=i*Q_HTR/N
end

Duplicate i=1;N
  h_H_HTR[i+1]=h_H_HTR[i]+Q_HTR/(m*N)
  T_H_HTR[i+1]=Temperature(CarbonDioxide;P=P_H_HTR;h=h_H_HTR[i+1])
end

Duplicate i=1;N
  h_C_HTR[i+1]=h_C_HTR[i]+Q_HTR/(m*N)
  T_C_HTR[i+1]=Temperature(CarbonDioxide;P=P_C_HTR;h=h_C_HTR[i+1])
end

Duplicate i=1;N+1
  delta_TC_HTR[i]=T_H_HTR[i]-T_C_HTR[i]
end

Duplicate i=1;N
  C_H_HTR[i]=m*(h_H_HTR[i+1]-h_H_HTR[i])/(T_H_HTR[i+1]-T_H_HTR[i])
  C_C_HTR[i]=m*(h_C_HTR[i+1]-h_C_HTR[i])/(T_C_HTR[i+1]-T_C_HTR[i])
end

Duplicate i=1;N
  eff_HTR[i]=Q_HTR/(N*min(C_H_HTR[i];C_C_HTR[i])*(T_H_HTR[i+1]-T_C_HTR[i]))
  NTU_HTR[i]=HX('counterflow';eff_HTR[i];C_H_HTR[i];C_C_HTR[i];'NTU')
  UA_HTR[i]=NTU_HTR[i]*min(C_H_HTR[i];C_C_HTR[i])
end

UA_HTR=sum(UA_HTR[i];i=1;N)

{LTR}
T_Cin_LTR=T_8
T_Cout_LTR=T_9
T_Hin_LTR=T_5
T_Hout_LTR=T_6
P_C_LTR=P_max
P_H_LTR=P_min
h_Cin_LTR=h_8
h_Cout_LTR=h_9
h_Hin_LTR=h_5
h_Hout_LTR=h_6

Q_LTR=m*(h_Hin_LTR-h_Hout_LTR)
Q_LTR2=SR*m*(h_Cout_LTR-h_Cin_LTR)
T_H_LTR[1]=T_Hout_LTR
T_C_LTR[1]=T_Cin_LTR
h_H_LTR[1]=h_Hout_LTR
h_C_LTR[1]=h_Cin_LTR

Duplicate i=1;N
  Q_LTR[i]=i*Q_LTR/N
end

Duplicate i=1;N

```

```

    h_H_LTR[i+1]=h_H_LTR[i]+Q_LTR/(m*N)
    T_H_LTR[i+1]=Temperature(CarbonDioxide;P=P_H_LTR;h=h_H_LTR[i+1])
end

Duplicate i=1;N
    h_C_LTR[i+1]=h_C_LTR[i]+Q_LTR/(SR*m*N)
    T_C_LTR[i+1]=Temperature(CarbonDioxide;P=P_C_LTR;h=h_C_LTR[i+1])
end

Duplicate i=1;N+1
    delta_TC_LTR[i]=T_H_LTR[i]-T_C_LTR[i]
end
Duplicate i=1;N
    C_H_LTR[i]=m*(h_H_LTR[i+1]-h_H_LTR[i])/(T_H_LTR[i+1]-T_H_LTR[i])
    C_C_LTR[i]=SR*m*(h_C_LTR[i+1]-h_C_LTR[i])/(T_C_LTR[i+1]-T_C_LTR[i])
end

Duplicate i=1;N
    eff_LTR[i]=Q_LTR/(N*min(C_H_LTR[i];C_C_LTR[i])*(T_H_LTR[i+1]-T_C_LTR[i]))
    NTU_LTR[i]=HX('counterflow';eff_LTR[i];C_H_LTR[i];C_C_LTR[i];'NTU')
    UA_LTR[i]=NTU_LTR[i]*min(C_H_LTR[i];C_C_LTR[i])
end

UA_LTR=sum(UA_LTR[i];i=1;N)

UA_REC=UA_HTR+UA_LTR

```

C.2 Partial Cooling Cycle EES Code

{UNITS: Pressure (MPa), Temperature (°C), Mass (kg), Energy (kJ)}

{INPUT DATA}

```

CIT= {°C}
TIT= {°C}
P_max= {MPa}
PR= {-}
RPR= {-}
eta_C= {-}
eta_T= {-}
epsilon_HTR= {-}
epsilon_hot= {-}
W_net= {kW}
N= {-}

```

{THERMODYNAMIC CYCLE}

```

P_min=P_max/PR
P_int=(P_max+P_min)/2
RPR=(P_max/P_int-1)/(PR-1)

T_1=TIT
P_1=P_max
h_1=Enthalpy(CarbonDioxide;T=T_1;P=P_1)
s_1=Entropy(CarbonDioxide;T=T_1;P=P_1)

P_2s=P_int
s_2s=s_1
h_2s=Enthalpy(CarbonDioxide;P=P_2s;s=s_2s)

eta_T=(h_1-h_2)/(h_1-h_2s)
P_2=P_int
T_2=Temperature(CarbonDioxide;P=P_2;h=h_2)

T_3=TIT

```

$P_3 = P_{int}$
 $h_3 = \text{Enthalpy}(\text{CarbonDioxide}; T=T_3; P=P_3)$
 $s_3 = \text{Entropy}(\text{CarbonDioxide}; T=T_3; P=P_3)$

$P_{4s} = P_{min}$
 $s_{4s} = s_3$
 $h_{4s} = \text{Enthalpy}(\text{CarbonDioxide}; P=P_{4s}; s=s_{4s})$

$\eta_{T_3} = (h_3 - h_{4s}) / (h_3 - h_{4s})$
 $P_4 = P_{min}$
 $T_4 = \text{Temperature}(\text{CarbonDioxide}; P=P_4; h=h_4)$

$P_6 = P_{min}$
 $\epsilon_{hot} = (h_4 - h_6) / (h_4 - \text{Enthalpy}(\text{CarbonDioxide}; T=T_{10}; P=P_6))$
 $T_6 = \text{Temperature}(\text{CarbonDioxide}; P=P_6; h=h_6)$

$T_7 = \text{CIT}$
 $P_7 = P_{min}$
 $h_7 = \text{Enthalpy}(\text{CarbonDioxide}; T=T_7; P=P_7)$
 $s_7 = \text{Entropy}(\text{CarbonDioxide}; T=T_7; P=P_7)$

$P_{8s} = P_{inter}$
 $s_{8s} = s_7$
 $h_{8s} = \text{Enthalpy}(\text{CarbonDioxide}; P=P_{8s}; s=s_{8s})$

$\eta_C = (h_{8s} - h_7) / (h_{8s} - h_7)$
 $P_8 = P_{inter}$
 $T_8 = \text{Temperature}(\text{CarbonDioxide}; P=P_8; h=h_8)$
 $s_8 = \text{Entropy}(\text{CarbonDioxide}; P=P_8; h=h_8)$

$T_9 = \text{CIT}$
 $P_9 = P_{inter}$
 $h_9 = \text{Enthalpy}(\text{CarbonDioxide}; T=T_9; P=P_9)$
 $s_9 = \text{Entropy}(\text{CarbonDioxide}; T=T_9; P=P_9)$

$P_{10s} = P_{max}$
 $s_{10s} = s_9$
 $h_{10s} = \text{Enthalpy}(\text{CarbonDioxide}; P=P_{10s}; s=s_{10s})$

$\eta_C = (h_{10s} - h_9) / (h_{10s} - h_9)$
 $P_{10} = P_{max}$
 $T_{10} = \text{Temperature}(\text{CarbonDioxide}; P=P_{10}; h=h_{10})$

$P_{12s} = P_{max}$
 $s_{12s} = s_8$
 $h_{12s} = \text{Enthalpy}(\text{CarbonDioxide}; P=P_{12s}; s=s_{12s})$

$\eta_C = (h_{12s} - h_8) / (h_{12s} - h_8)$
 $P_{12} = P_{max}$
 $T_{12} = \text{Temperature}(\text{CarbonDioxide}; P=P_{12}; h=h_{12})$

$T_{11} = T_{12}$
 $P_{11} = P_{12}$
 $h_{11} = h_{12}$

$T_{13} = T_{12}$
 $P_{13} = P_{12}$
 $h_{13} = h_{12}$

$P_5 = P_{min}$
 $\epsilon_{HTR} = (h_4 - h_5) / (h_4 - \text{Enthalpy}(\text{CarbonDioxide}; T=T_{13}; P=P_5))$
 $T_5 = \text{Temperature}(\text{CarbonDioxide}; P=P_5; h=h_5)$

```

h_14-h_13=h_4-h_5
P_14=P_max
T_14=Temperature(CarbonDioxide;P=P_14;h=h_14)

```

{CYCLE PERFORMANCE}

```
SR*(h_11-h_10)=h_5-h_6
```

```

W_HPT=m*(h_1-h_2)
W_LPT=m*(h_3-h_4)
W_MC=SR*m*(h_10-h_9)
W_RC=(1-SR)*m*(h_12-h_8)
W_PC=m*(h_8-h_7)
W_net=W_HPT+W_LPT-W_MC-W_RC-W_PC

```

```

Q_heat=m*(h_1-h_14)
Q_reheat=m*(h_3-h_2)
Q_in=Q_heat+Q_reheat

```

```
eta_th=W_net/Q_in*100
```

```
E_LTR=(h_5-h_6)/(h_5-Enthalpy(CarbonDioxide;T=T_10;P=P_6))
```

{HTR}

```

T_Cin_HTR=T_13
T_Cout_HTR=T_14
T_Hin_HTR=T_4
T_Hout_HTR=T_5
P_C_HTR=P_max
P_H_HTR=P_min
h_Cin_HTR=h_13
h_Cout_HTR=h_14
h_Hin_HTR=h_4
h_Hout_HTR=h_5

```

```

Q_HTR=m*(h_Hin_HTR-h_Hout_HTR)
Q_HTR2=m*(h_Cout_HTR-h_Cin_HTR)
T_H_HTR[1]=T_Hout_HTR
T_C_HTR[1]=T_Cin_HTR
h_H_HTR[1]=h_Hout_HTR
h_C_HTR[1]=h_Cin_HTR

```

```

Duplicate i=1;N
  Q_HTR[i]=i*Q_HTR/N
end

```

```

Duplicate i=1;N
  h_H_HTR[i+1]=h_H_HTR[i]+Q_HTR/(m*N)
  T_H_HTR[i+1]=Temperature(CarbonDioxide;P=P_H_HTR;h=h_H_HTR[i+1])
end

```

```

Duplicate i=1;N
  h_C_HTR[i+1]=h_C_HTR[i]+Q_HTR/(m*N)
  T_C_HTR[i+1]=Temperature(CarbonDioxide;P=P_C_HTR;h=h_C_HTR[i+1])
end

```

```

Duplicate i=1;N
  delta_TC_HTR[i]=T_H_HTR[i]-T_C_HTR[i]
end

```

```

Duplicate i=1;N
  C_H_HTR[i]=m*(h_H_HTR[i+1]-h_H_HTR[i])/(T_H_HTR[i+1]-T_H_HTR[i])
  C_C_HTR[i]=m*(h_C_HTR[i+1]-h_C_HTR[i])/(T_C_HTR[i+1]-T_C_HTR[i])
end

```

```

Duplicate i=1;N
  eff_HTR[i]=Q_HTR/(N*min(C_H_HTR[i];C_C_HTR[i]))*(T_H_HTR[i+1]-T_C_HTR[i])
  NTU_HTR[i]=HX('counterflow';eff_HTR[i];C_H_HTR[i];C_C_HTR[i];'NTU')
  UA_HTR[i]=NTU_HTR[i]*min(C_H_HTR[i];C_C_HTR[i])
end

```

```

UA_HTR=sum(UA_HTR[i];i=1;N)

```

```

{LTR}

```

```

T_Cin_LTR=T_10
T_Cout_LTR=T_11
T_Hin_LTR=T_5
T_Hout_LTR=T_6
P_C_LTR=P_max
P_H_LTR=P_min
h_Cin_LTR=h_10
h_Cout_LTR=h_11
h_Hin_LTR=h_5
h_Hout_LTR=h_6

```

```

Q_LTR=m*(h_Hin_LTR-h_Hout_LTR)
Q_LTR2=SR*m*(h_Cout_LTR-h_Cin_LTR)
T_H_LTR[1]=T_Hout_LTR
T_C_LTR[1]=T_Cin_LTR
h_H_LTR[1]=h_Hout_LTR
h_C_LTR[1]=h_Cin_LTR

```

```

Duplicate i=1;N
  Q_LTR[i]=i*Q_LTR/N
end

```

```

Duplicate i=1;N
  h_H_LTR[i+1]=h_H_LTR[i]+Q_LTR/(m*N)
  T_H_LTR[i+1]=Temperature(CarbonDioxide;P=P_H_LTR;h=h_H_LTR[i+1])
end

```

```

Duplicate i=1;N
  h_C_LTR[i+1]=h_C_LTR[i]+Q_LTR/(SR*m*N)
  T_C_LTR[i+1]=Temperature(CarbonDioxide;P=P_C_LTR;h=h_C_LTR[i+1])
end

```

```

Duplicate i=1;N
  delta_TC_LTR[i]=T_H_LTR[i]-T_C_LTR[i]
end

```

```

Duplicate i=1;N
  C_H_LTR[i]=m*(h_H_LTR[i+1]-h_H_LTR[i])/(T_H_LTR[i+1]-T_H_LTR[i])
  C_C_LTR[i]=SR*m*(h_C_LTR[i+1]-h_C_LTR[i])/(T_C_LTR[i+1]-T_C_LTR[i])
end

```

```

Duplicate i=1;N
  eff_LTR[i]=Q_LTR/(N*min(C_H_LTR[i];C_C_LTR[i]))*(T_H_LTR[i+1]-T_C_LTR[i])
  NTU_LTR[i]=HX('counterflow';eff_LTR[i];C_H_LTR[i];C_C_LTR[i];'NTU')
  UA_LTR[i]=NTU_LTR[i]*min(C_H_LTR[i];C_C_LTR[i])
end

```

```

UA_LTR=sum(UA_LTR[i];i=1;N)

```

```

UA_REC=UA_HTR+UA_LTR

```

Appendix D Models of CSP Plants in Thermoflex

The layouts of the CSP plants modelled in Thermoflex for the different scenarios are presented in this appendix.

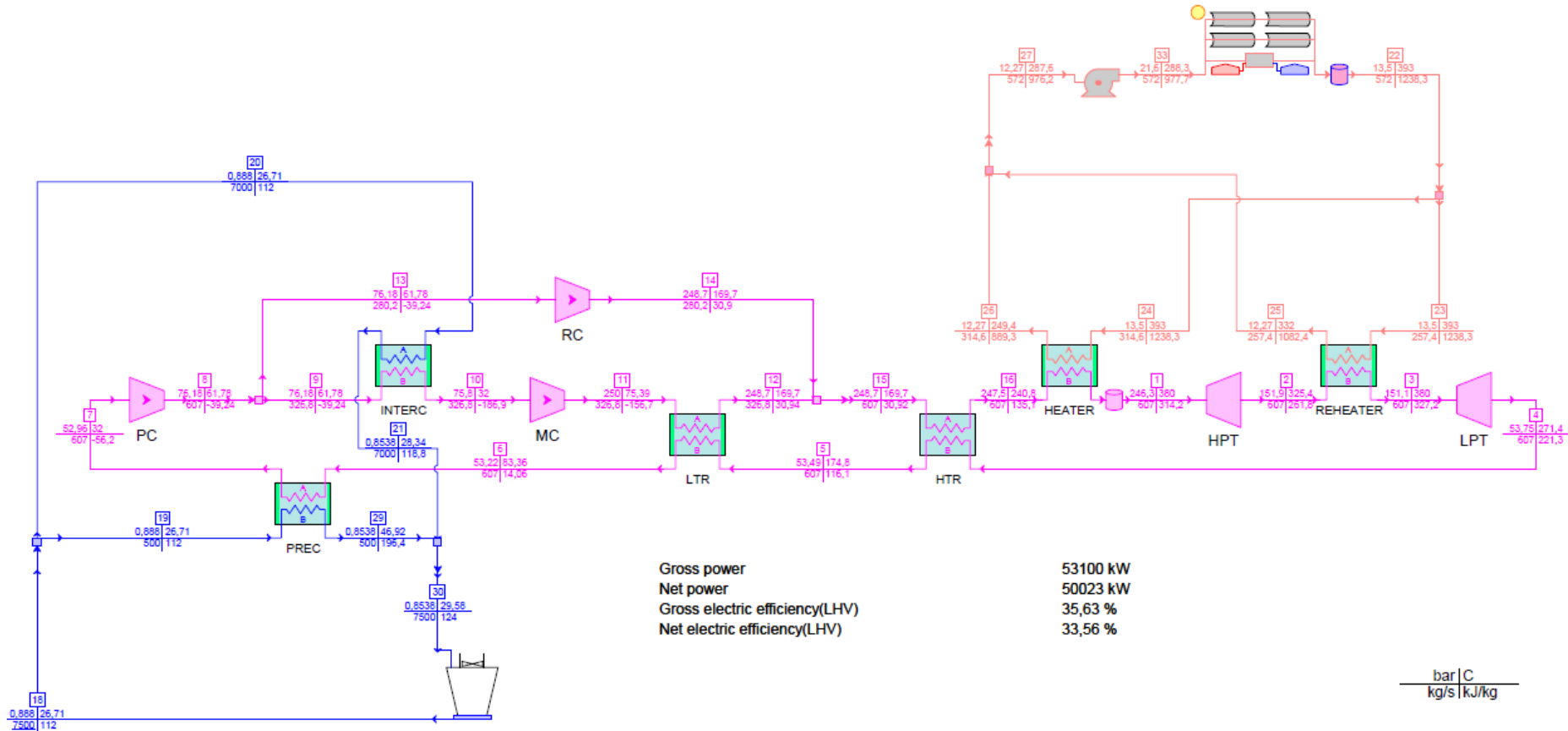


Figure A-8. Model of parabolic trough CSP plant with s-CO₂ partial cooling cycle in Thermoflex (scenario 1)

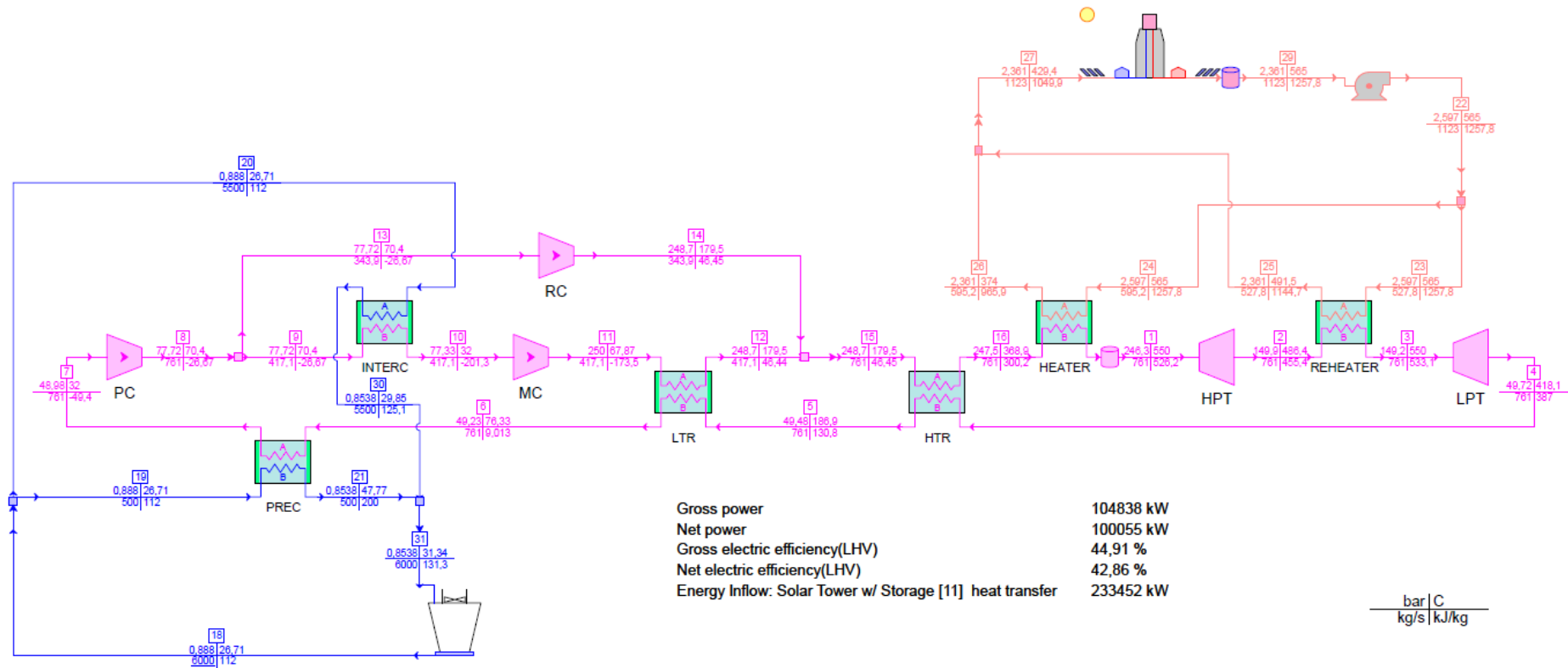


Figure A-9. Model of central tower CSP plant with s-CO₂ partial cooling cycle in Thermoflex (scenario 2)

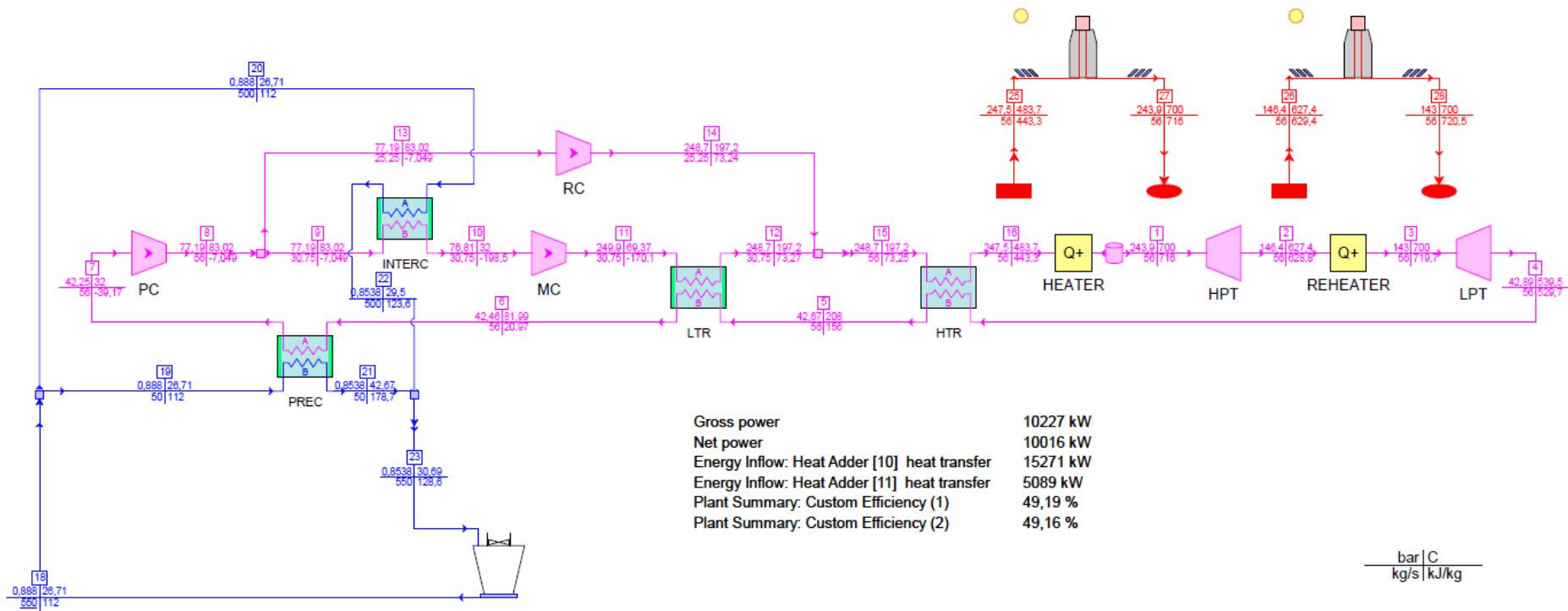


Figure A-10. Model of modular tower CSP plant with wet cooling and s-CO₂ partial cooling cycle in Thermoflex (scenario 3)

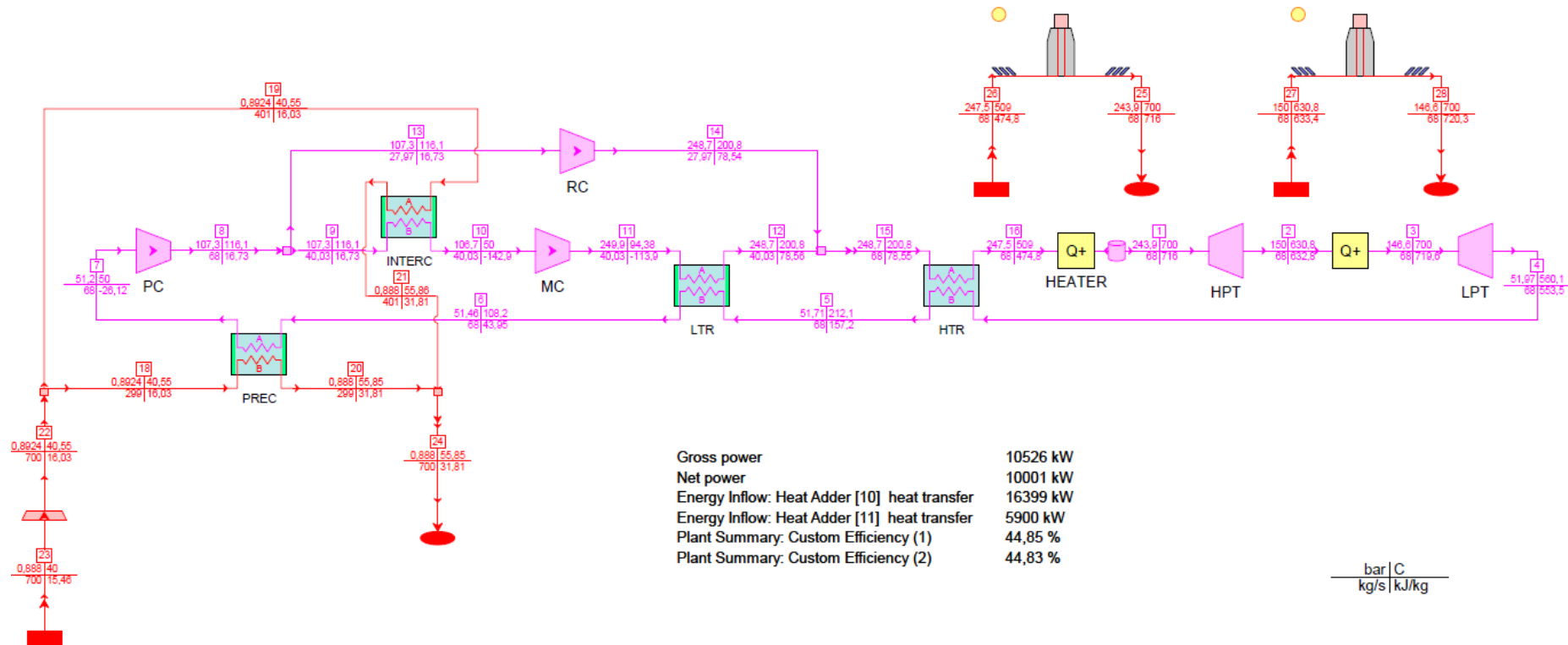


Figure A-11. Model of modular tower CSP plant with dry cooling and s-CO₂ partial cooling cycle in Thermoflex (scenario 4)

Appendix E Receiver for Direct Heating of s-CO₂

This appendix includes a simplified analysis of the pressure drops in a tubular receiver that could be used for direct heating of s-CO₂ in the scenarios 3 and 4. It is based on the analysis of Neises *et al.* [25] and it is assumed that the proposed design of the tubes is valid for these conditions. A tubular receiver consists of thinned-wall tubes arranged as a cylinder. The heat transfer fluid (HTF) is heated by the solar radiation as it passes through multiple panels.

The characteristics of the tubes that form the receiver are shown in Table A-1.

Table A-1. Tubes parameters [25]

Diameter	12 mm
Thickness	2.5 mm
Length	4.1 m
Material	Haynes 230
Roughness	0.045 mm
Heat Absorbed	14.76 kW

In scenarios 3 and 4, a combined receiver in a single tower would be used for the heater and reheater. However, this requires to determine precisely the design of the receiver. As a simplification, the pressure drops are calculated as friction losses only in the heater, since it is the main heat input. The expression of friction pressure losses corresponds to Darcy-Weisbach equation for a cylindrical pipe:

$$\Delta P = f \frac{L}{D} \frac{\rho v^2}{2} \quad (\text{A-9})$$

The pressure drops cover from the inlet to the outlet of the heater, where a TIT of 700°C is reached. The mass flowrate of the HTF is divided into the number of tubes per panel and it is assumed that the receiver has a height equal to the length of the tubes, eight panels and two symmetrical paths for the fluid. This means a total length for pressure losses of four times the length of the tubes. In addition, the number of tubes is determined as the heat input in the heater divided by the allowable heat absorbed per tube. All these assumption result in the following parameters and pressure drops (Table A- 2).

Table A- 2. Pressure drops in heaters of scenario 3 and 4

Parameter	Scenario 3	Scenario 4
Number of tubes	1040	1120
Number of tubes per panel	130	140
Mass flowrate per panel	0.215 kg/s	0.243 kg/s
Inlet Temperature	483.7°C	509°C
Inlet pressure	247.5 bar	247.5 bar
Pressure drop	77.05 bar	100.18 bar
%Pressure drop	31.1%	40.5%